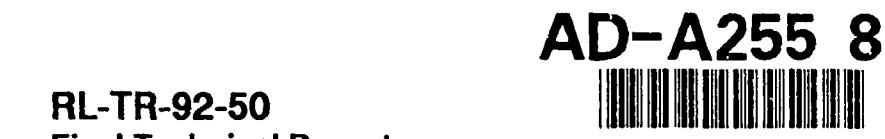

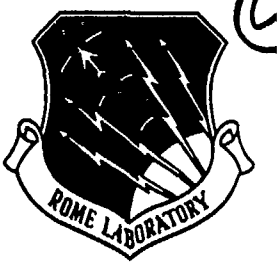


RL-TR-92-50
Final Technical Report
May 1992

# FAST OPTOELECTRONIC SWITCHING PROCESSES IN SURFACE-EMITTING SEMICONDUCTOR LASERS AND NONLINEAR ETALONS

University of New Mexico

John G. McInerney

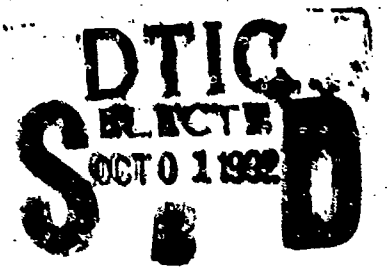


*APPROVED FOR PUBLIC RELEASE; DISTRIBUTION UNLIMITED.*



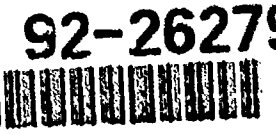

Rome Laboratory
Air Force Systems Command
Griffiss Air Force Base, NY 13441-5700

This report has been reviewed by the Rome Laboratory Public Affairs Office (PA) and is releasable to the National Technical Information Service (NTIS). At NTIS it will be releasable to the general public, including foreign nations.

RL-TR-92-50 has been reviewed and is approved for publication.

APPROVED: Kenneth Vaccaro

KENNETH VACCARO
Project Engineer

FOR THE COMMANDER: Harold Roth

HAROLD ROTH, Director
Electromagnetics and Reliability Directorate

If your address has changed or if you wish to be removed from the Rome Laboratory mailing list, or if the addressee is no longer employed by your organization, please notify RL(ERO ) Hanscom AFB MA 01731-5000. This will assist us in maintaining a current mailing list.

Do not return copies of this report unless contractual obligations or notices on a specific document require that it be returned.

# REPORT DOCUMENTATION PAGE

Form Approved
OMB No. 0704-0188



| 1. AGENCY USE ONLY (Leave Blank) | 2. REPORT DATE | 3. REPORT TYPE AND DATES COVERED |
|---|---|---|
| | May 1992 | Final Sep 89 - Sep 91 |

**4. TITLE AND SUBTITLE**
FAST OPTOELECTRONIC SWITCHING PROCESSES IN SURFACE-EMITTING SEMICONDUCTOR LASERS AND NONLINEAR ETALONS

**5. FUNDING NUMBERS**
C - F19628-89-K-0037
PE - 61102F
PR - 2306
TA - J2
WU - 68

**6. AUTHOR(S)**
John G. McInerney

**7. PERFORMING ORGANIZATION NAME(S) AND ADDRESS(ES)**
University of New Mexico
FEEE Building, Room 125
Albuquerque NM 87131

**8. PERFORMING ORGANIZATION REPORT NUMBER**
N/A

**9. SPONSORING/MONITORING AGENCY NAME(S) AND ADDRESS(ES)**
Rome Laboratory (ERO)
Hanscom AFB MA 01731-5000

**10. SPONSORING/MONITORING AGENCY REPORT NUMBER**
RL-TR-92-50

**11. SUPPLEMENTARY NOTES**
Rome Laboratory Project Engineer: Kenneth Vaccaro/ERO/(617) 377-4921

**12a. DISTRIBUTION/AVAILABILITY STATEMENT**
Approved for public release; distribution unlimited.

**12b. DISTRIBUTION CODE**

**13. ABSTRACT** (Maximum 200 words)

We describe theoretical and experimental research on optoelectronic switching processes in GaAs/AlGaAs multiple quantum well etalons, where the quantum wells are spaced by one-half the optical wavelength at which the structure is designed to operate. Results have been obtained with the quantum wells pumped above threshold (i.e. the structure behaves as a surface-emitting laser) and below threshold (when it behaves as a saturable absorber with feedback). In the former case, high-speed (10 ps impulse response) switching has been demonstrated, but the threshold is relatively high. Some suggestions for more efficient switching are made. In the latter case, a detailed theoretical model has been developed which demonstrates the potential advantages and disadvantages of absorptive bistable optical switching in half-wave-periodic MQW etalons over the conventional non-resonant MQW or bulk structures. The initial experiments were promising but hampered by materials growth and uniformity problems. We include several specific recommendations for additional experiments to complete our investigations of the below-threshold switching regime, as well as extension to 2-D switch arrays, new research directions and applications such as time-division multiplexing.

**14. SUBJECT TERMS**
Surface-emitting lasers, bistable optical switches, III-V semiconductor quantum well devices

**15. NUMBER OF PAGES**
44

**16. PRICE CODE**

| 17. SECURITY CLASSIFICATION OF REPORT | 18. SECURITY CLASSIFICATION OF THIS PAGE | 19. SECURITY CLASSIFICATION OF ABSTRACT | 20. LIMITATION OF ABSTRACT |
|---|---|---|---|
| UNCLASSIFIED | UNCLASSIFIED | UNCLASSIFIED | UL |

# 1 INTRODUCTION

## 1.1 Vertical-cavity structures

Vertical-cavity semiconductor structures are extremely promising for optoelectronics. In these structures, light propagates in a direction normal to the wafer surface, as opposed to the more conventional in-plane propagation. Whereas in-plane structures are suitable for guided-wave applications and are limited to one-dimensional array expansion, vertical-cavity geometries are most convenient for free-space propagation and are capable of extension into two-dimensional arrays. They are therefore particularly appropriate for optical signal and image processing.

In this project we are concerned with optical switching in active and passive vertical-cavity semiconductor structures. The ultimate aim is to understand the physics, technology and practicalities of fast (nanosecond or better), efficient optical switch arrays. We define active structures as those which possess internal gain, that is lasers or optical amplifiers: we have concentrated on vertical-cavity surface-emitting lasers. Passive switches do not possess gain but are important in situations where minimal power consumption and switching thresholds are desired. We have considered multiple quantum well etalons which exhibit absorptive optical bistability.

From the beginning, therefore, this research project divides into two streams, but there are many physical and technological similarities between the active and passive device structures, so it is natural to consider them in tandem.

## 1.2 RPG and RPA Media

In 1987 our research group at the University of New Mexico began to consider the physics of semiconductor heterostructures containing multiple quantum wells with optical periodicity, with a view to studying correlated emission. We quickly realized that half-wave-periodic structures in which the gain elements overlapped with the antinodes of an optical standing wave would provide enhanced gain at a chosen wavelength and in a specific direction, effectively suppressing the amplified spontaneous emission (ASE) which had bedeviled the vertical cavity surface-emitting lasers previously demonstrated. Figure 1 shows the resulting resonant periodic gain (RPG) medium. The effective gain for an optical wave resonating in such a structure along the z-axis (*i.e.* normal to the planes of the quantum wells) is weighted by the standing wave intensity sine-squared pattern, and is therefore given by [1]

$$G(\lambda) = \int g(z)\sin^2(kz)dz, \qquad (1)$$

where $k(z) = 2\pi n(\lambda)/\lambda$ is the propagation constant, $g(z)$ is the axial distribution of the gain per unit length (which in our structure consists of a series of top-hat functions corresponding to the thin gain sheets) and the integral is

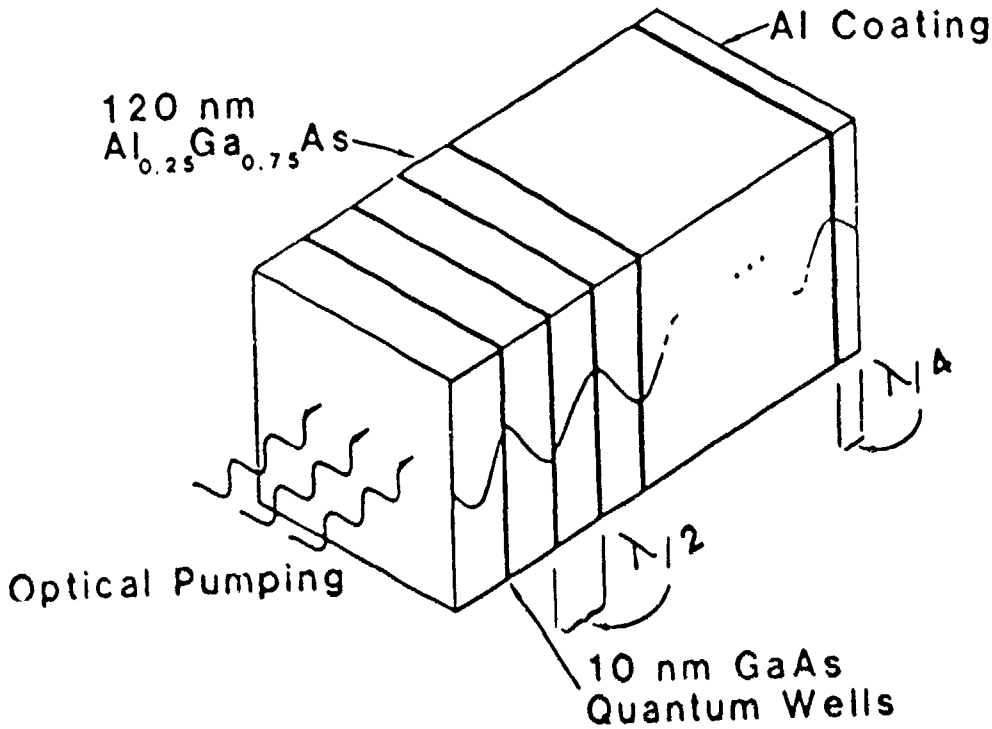


**FIGURE 1**

Schematic of early RPG-VCSEL structure showing half-wave-spaced quantum wells aligned with the antinodes of the optical standing wave field.

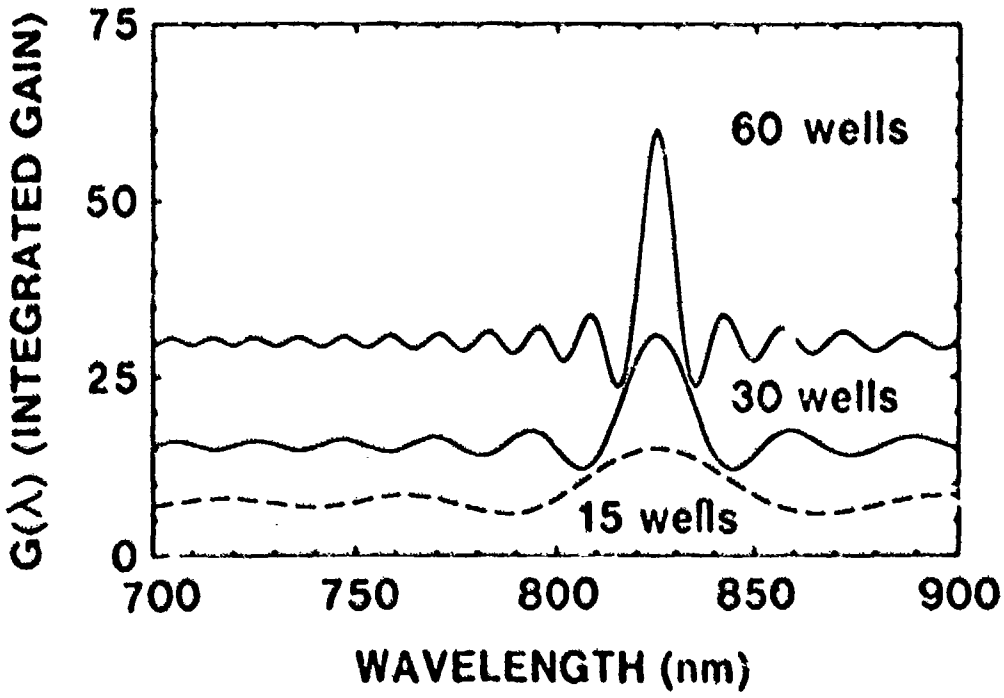


**FIGURE 2**

Calculated effective gain spectra (assuming a very broad material gain spectrum) for waves propagating along the normal to a RPG structure, demonstrating gain enhancement by a factor of two on resonance.

taken over the entire normal length L of the structure. We see in Figure 2 that a wave resonant with the quantum well periodicity (*i.e.* the QW spacing = $p\lambda/2$, $p$ a positive integer) can experience twice as much gain as a wave which is non-resonant. Similar calculations show that a resonant wave propagating normally to the quantum wells experiences twice as much gain as a wave propagating in another direction. Hence the usual problem of lateral amplified spontaneous emission (ASE) is greatly reduced in these RPG media. However, they are sensitive to wavelength, material composition and positioning of the quantum wells in the resonator.

The same argument holds true for optimization of the optical absorption: when the RPG medium is pumped below threshold, a wave propagating normally whose wavelength is resonant with the quantum well spacing will experience twice as much absorption as a wave with a non-resonant wavelength and/or a different direction of propagation. In effect, we are placing the absorbers where they can do the most good. We refer to this medium as a RPA (resonant periodic absorption) structure, by analogy with the RPG structure, even though the two structures are almost identical in construction. ASE is not a problem here, but the switching threshold should be lower and the contrast between saturable and unsaturable losses should be considerably better for the RPA switch, resulting in improved on/off contrast.

The benefits likely to result from the RPG/RPA concept carry a price, in that the structure requires careful matching of the design wavelength with a cavity longitudinal mode and with a gain/absorption peak (usually at the $n=1$ quantum well subband transition for lasers, or an excitonic resonance for absorbers) and also careful choice of the dimensions and compositions so that the antinodes of the standing wave optical field overlap spatially with the quantum wells.

We note in passing that any series of localized gain or absorption sheets can be used to implement the RPG/RPA concept: single quantum wells, groups of closely-spaces quantum wells, or quasi-bulk thin films. The concept is meaningful provided that the sheets are thin compared with the optical wavelength.

### 1.3 Vertical-cavity surface-emitting lasers (VCSELs)

Vertical cavity surface-emitting semiconductor lasers (VCSELs) [1,2] offer considerable promise for development of high-power laser arrays, highly parallel optical interconnections, and spatially coherent sources for free-space illumination, communication and ranging. VCSELs should lend themselves particularly well to 2-D arrays and large-aperture emitters with good beam quality (edge-emitting semiconductor lasers are notoriously poor in this respect). Moreover, the fabrication should be simplified in that planar processes are used exclusively.

Following the formulation of the notion of a periodic gain medium in a high-Q optical cavity, we validated the RPG concept by optical pumping experiments using dye lasers. These first samples quickly led to optimized

devices with optical cavities formed by pairs of multilayer epitaxial reflectors with reflectivities in excess of 99%. These devices were entirely grown by metal-organic vapor phase epitaxy (MOVPE) at UNM, and required no further processing for optically pumped lasing. A typical RPG-VCSEL structure is illustrated in Figure 3, in which the number of layers has been reduced for clarity. In this report we describe the preliminary results of our studies of the switching properties of these RPG-VCSEL structures above and below threshold.

### 1.4 Electrically pumped VCSELs

The RPG-VCSEL is an extremely versatile device: it can be pumped by transverse or longitudinal electrical injection as well as by illumination with other lasers or even by relatively incoherent sources such as diode laser arrays [3] and possibly by several such sources in combination. Transverse electrical injection, which was first demonstrated at UNM, suffers from poor in-plane carrier transport and hence very low laser quantum efficiency (a few percent [4]). VCSELs have been made to lase by longitudinal electrical injection at several laboratories, but this scheme also suffers from carrier transport problems since the electrons and holes must traverse many barriers as they drift at right angles to the epitaxial planes.

To our knowledge, the best results obtained using electrically injected VCSELs have recently been obtained at UNM. Our best devices have turn-on voltages of $<2.5$ V and series resistances of $\sim 25\ \Omega$ for pumped spots 20 $\mu$m in diameter; they consist of multiple graded and doped mirror and spacer layers with proton implant isolation, have threshold currents of 5 mA or so and can produce $\sim 1$ mW of optical power without any special heat sinking [5]. The availability of such high-quality injection-pumped RPG-VCSELs makes hybrid active or passive optoelectronic switching possible, where the switch is biased electrically and is triggered optically. These impressive achievements open up new possibilities for future research and development of hybrid electrical/optical switching mechanism, as outlined in Section 5 of this report.

## 2 OPTICAL SWITCHING IN RPG LASERS ABOVE THRESHOLD

### 2.1 Sample design and fabrication

Typical vertical-cavity surface-emitting semiconductor lasers (VCSELs) and nonlinear etalons fabricated as part of this work have consisted of RPG media sandwiched between multilayer epitaxial highly-reflecting stacks. The number of epitaxial layers in such structures can easily exceed 100, so it is essential to have suitable computational design tools: designing RPG/RPA wafers can be counter-intuitive. Our approach is to use a matrix model for optical propagation through these multilayer structures, similar in concept to the usual methods for designing multilayer dielectric films for coating optical components. The first iteration assumed real indices, neglecting the effects of gain/absorption or material dispersion. This is usually an adequate though crude

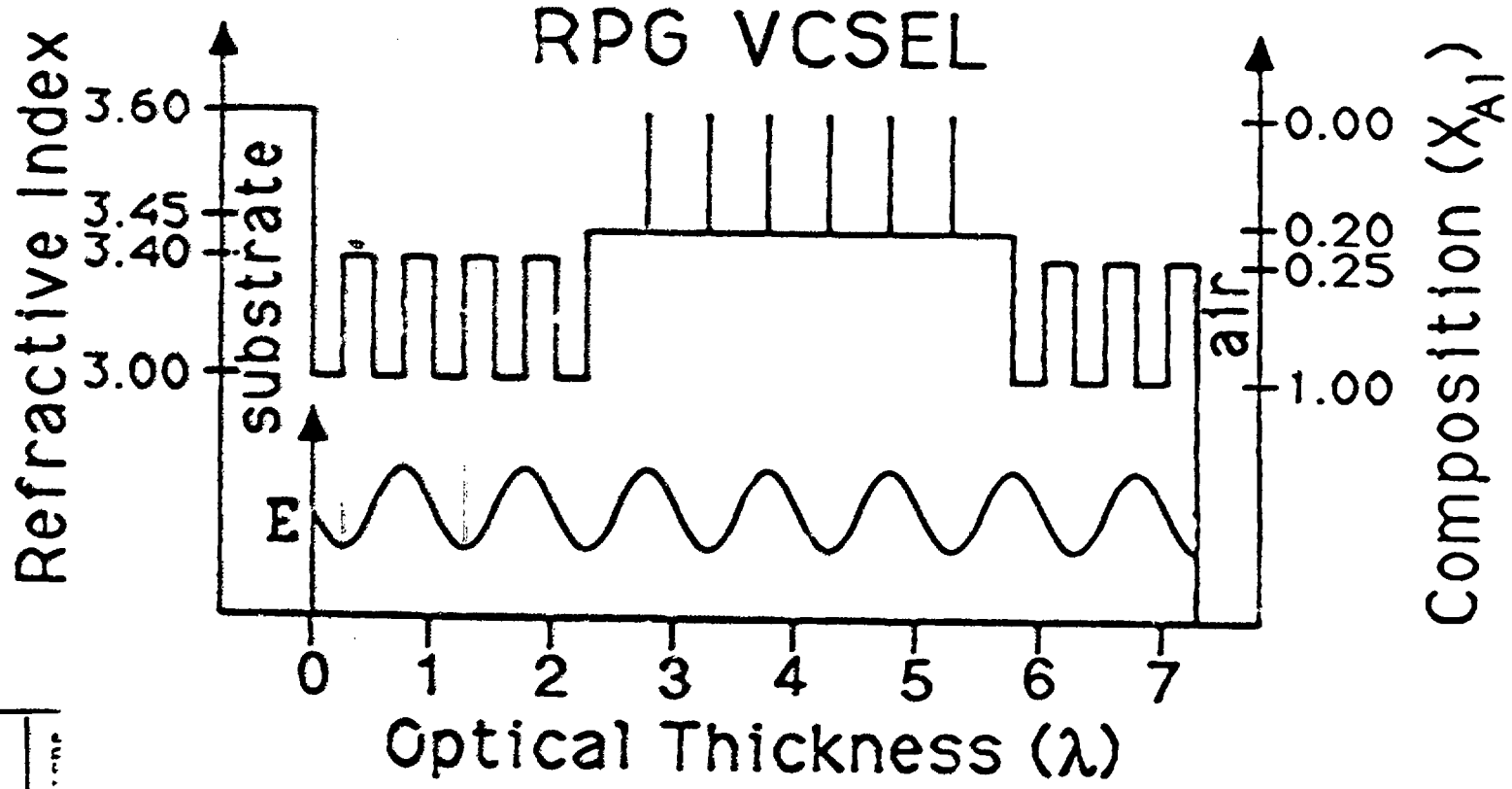


**FIGURE 3**

Simplified diagram of a modern GaAs/AlGaAs RPG-VCSEL designed for optical pumping, showing optimal location of the optical standing wave in the structure. The number of layers has been reduced for clarity.

approximation for lasers and nonlinear etalons; however, it is a good approximation for RPG/RPA structures in which the overall gain/absorption is quite weak, being confined to the quantum wells. Also, the structures themselves are highly wavelength-selective: the optical periodicity of the quantum wells and the multilayer stacks induces dispersion which is much greater than the material dispersion.

Using this model, we have plotted reflectivity spectra for single multilayer mirrors and phase resonances for complete empty and filled optical cavities (*i.e.* for pairs of mirrors without and with enclosed gain/absorbing media). A typical calculated reflectivity spectrum is shown in Figure 4, which showed good agreement with a spectrum measured experimentally using a spectrophotometer. The following structures were designed:

GaAs/GaAlAs RPG VCSELs for optical pumping at 740 nm;
GaAs/GaAlAs RPG VCSELs for optical pumping at 800 nm;
pseudomorphic InGaAs/GaAs RPG VCSELs for optical pumping at 800 nm;
GaAs/GaAlAs RPA etalons without epitaxial reflectors.

The first three wafers were destined for above- and below-threshold switching, while the last was designed to study saturation of excitonic absorption in the quantum wells. We are now revising our model to study structures whose layers are graded along the optical axis for efficient pumping by longitudinal carrier injection, a refinement which will require more complicated finite-element or Fourier transform propagators.

## 2.2 Optimized pulsed and CW optical pumping

For efficient switching of semiconductor lasers and optical amplifiers, our prior experience has shown that it is highly desirable to operate with a steady bias close to the lasing or switching threshold. Accordingly, experiments were conducted to determine the optimal configurations for optical pumping of these devices. An important achievement of this research was efficient diode laser pumping of RPG-VCSELs.

Various GaAs/GaAlAs samples were designed (*cf.* Section 2.1 above) and grown by MOCVD in our laboratories. In an early experiment, standard double-heterostructure, non-resonant multiple quantum well (NR-MQW) and resonant periodic gain multiple quantum well (RPG-MQW) wafers were compared for optical pumping efficiency. These comparative measurements clearly indicated the advantage of the RPG concept for VCSELs: the device with the bulk GaAs active region failed to lase even in pulsed mode (7 ns, 10 Hz) even up to the optical damage threshold of ~5 MW $cm^{-2}$ on the sample surface at the pump wavelength of 680 nm. The NR-MQW samples lased erratically in pulsed mode close to the damage threshold but with relatively high thresholds and poor efficiencies. The RPG-MQW devices lased with thresholds and efficiencies a factor of two or so better than the nonresonant samples, as expected.

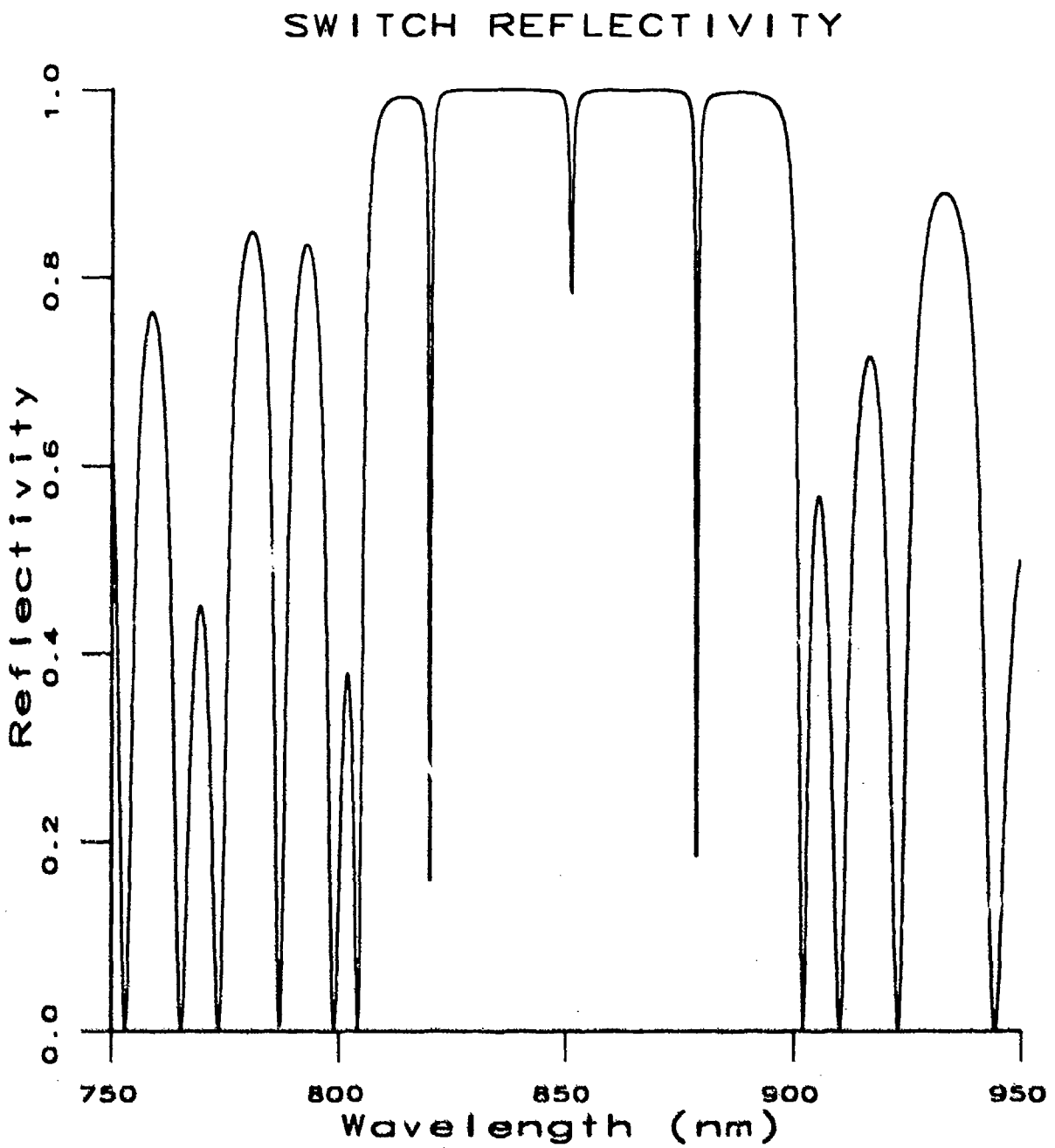


**FIGURE 4**

Calculated reflectivity spectrum for a RPG-VCSEL: the magnitude and position of the dip corresponding to the resonator mode must be chosen carefully.

By testing these samples, using CW dye laser pumping and measuring the output powers and optical spectra, we determined the optimum pumping wavelength for minimum threshold and maximum efficiency. For the first RPG structures grown, this was in the range 730-750 nm (see Figure 5). Improved structures with very high end mirror reflectivities (> 99.5%) lased continuously and efficiently at room temperature: typical thresholds were 20-30 mW CW absorbed pump power for a circular pumped spot ~10 μm in diameter. The best thresholds were just over 10 mW but these results were obtained only at a few spots on each wafer. The optical power conversion efficiencies were excellent, typically 20-40% when thermal saturation occurred at ~30 mW output for free-standing samples with no special heat sinking (Figure 6).

## 2.3 Optical pumping of VCSELs using edge-emitting diode lasers

For the next set of experiments, diode laser arrays emitting at 740 nm were specially fabricated and used to pump the RPG-MQW surface-emitting lasers with excellent results: electrical-to-optical power conversion efficiencies were more than 5% (most losses occurred in the optical coupling of the pump power), external quantum efficiencies were as high as 70% and pump-limited power outputs as high as 10 mW in a single 6 μm near-field spot. Typical spectra showed single longitudinal mode operation (as expected, given the short cavity lengths of a few μm) and nearly single mode outputs to almost 10 mW, with instrument-limited spectral widths of ~0.01-0.03 nm. Clearly these RPG-VCSELs have very good optical properties, suitable for further research into their optical switching properties, although the variations in laser properties across the wafers' surfaces will need to be reduced when large-area emission or uniform arrays will be required.

Another technological limitation was availability of pump power and poor beam quality from diode laser pump arrays at 740 nm. Due to continued difficulties in obtaining special crystal growth runs to fabricate lasers at this wavelength, we recalibrated our designs to use diode laser pumping at more conventional wavelengths (780-820 nm). These samples are due to be grown in early 1992. In the meantime, optical pumping experiments are continuing using dye and titanium:sapphire laser sources.

## 2.4 Transverse mode instabilities in VCSELs and prospects for fast switching

A significant problem in VCSELs is their extremely high Fresnel numbers

$$F = na^2/\lambda L \qquad (2)$$

where $a$ is the diameter of the lasing spot and $L$ is the overall cavity length. The Fresnel number expresses the transverse mode selectivity of a resonator: larger $F$ means lower selectivity. In edge-emitting semiconductor lasers $a$ is a few μm and $L$ is a few hundred μm, whereas in a VCSEL $a$ is tens or hundreds of μm and $L$ is only a

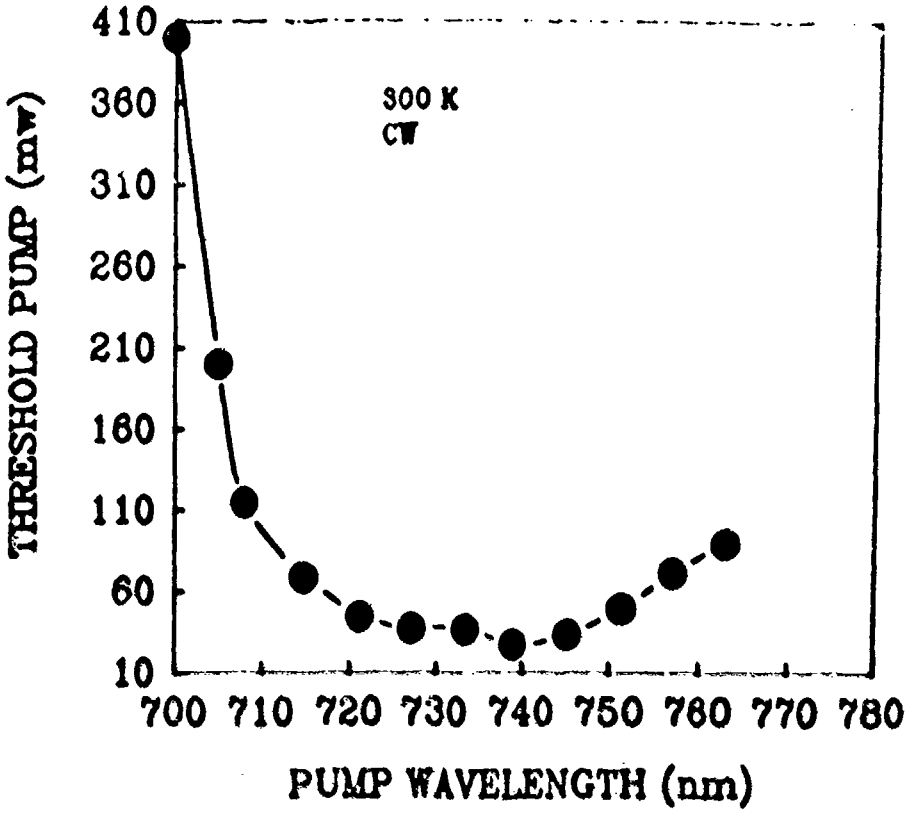


**FIGURE 5**

Experimentally measured threshold for a typical optically pumped RPG-VCSEL as a function of pump wavelength. The threshold rises at wavelengths shorter than 720 nm because of increasing pump absorption in the outer (mirror) layers; it rises at wavelengths longer than 750 nm because of decreasing absorption in the spacers between quantum wells.

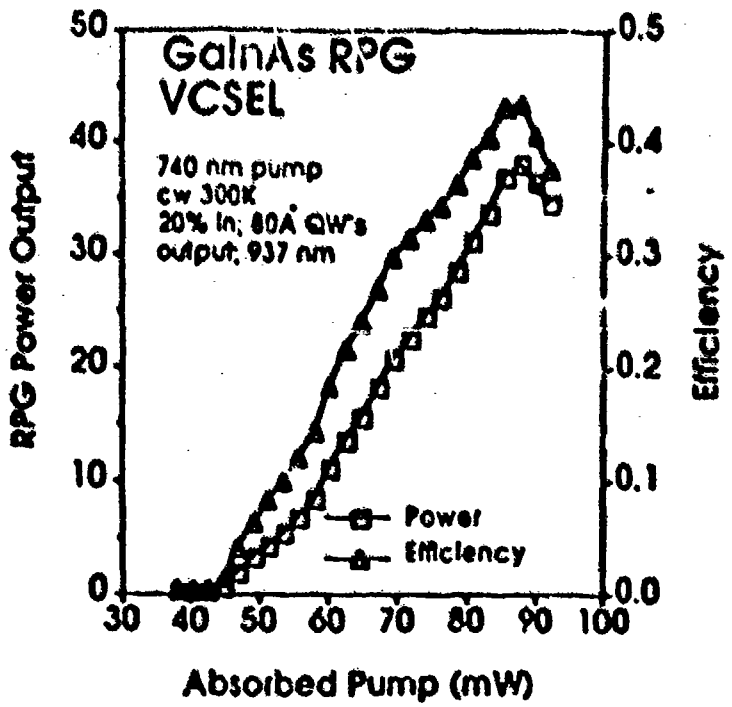


**FIGURE 6**

Measured power output and optical pumping efficiency for CW InGaAs/AlGaAs RPG-VCSEL at room temperature; the sample was free-standing, without any special heat sinking, and the saturation in both curves was due to thermal effects.

few $\mu$m. The Fresnel numbers for surface-emitters are therefore three or four orders of magnitude greater than those for edge-emitters, and VCSELs tend to be multi-transverse mode at output powers of $\sim$1 mW or more.

One consequence of large F-values is that VCSELs can exhibit instabilities as the transverse mode spectra change: as the output power is increased, kinks in the input-output characteristics occur which are accompanied by intensity and wavelength fluctuations in the laser output. We have observed such instabilities in several VCSELs with optical and electrical pumping, and in one sense they represent a considerable nuisance. However, we also believe that this phenomenon may provide opportunities for ultrafast optical switching, as discussed later.

Even when transverse mode instabilities are absent, multi-mode operation is still deleterious to applications such as fiber coupling and long-distance free-space propagation. Figure 7(a) shows the near-field, far-field and optical spectrum from a InGaAs/AlGaAs RPG-VCSEL at 2 mW output; Figure 7(b) shows the same curves at 15 mW output. Since single transverse mode VCSELs are highly desirable, we are considering various transverse mode selection geometries such as external cavities, saturable absorbers, and spatial modulation of the mirror reflectivities.

### 2.5 Gigahertz modulation of the diode-pumped RPG-VCSEL

Because the VCSEL can be pumped by an edge-emitting diode laser, it is convenient to modulate the VCSEL simply by modulating the pump laser. When the pump laser was pre-biased to threshold, the VCSEL exhibited a linear modulation response to 1.1 GHz, this limit being imposed by the available signal generators and amplifiers. This result indicates that sub-nanosecond response times should be obtained in optical switching, a conjecture which was verified in the next series of experiments.

### 2.6 Picosecond optical pumping

A set of MOCVD-grown GaAs/GaAlAs RPG-VCSEL samples with 20 quantum wells and epitaxial multilayer high-reflectivity stacks with R=0.995 and 0.999 was pumped by light from a synchronously-pumped mode-locked dye laser which generated 4 ps pulses at 82 MHz repetition rate, in a wavelength range from 650 to 750 nm. The shorter wavelength pump pulses were absorbed in the epitaxial mirror stacks, and the resulting luminescence then pumped the active region after some delay ($\sim$1 ns). Longer wavelengths (730-750 nm) were chosen for most efficient optical pumping by direct absorption in the active region, which also resulted in considerably shorter switch-on delays ($\sim$20 ps). By autocorrelation and by cross-correlation with pump pulses, we have determined the output pulse width and symmetry. The best result was 13 ps FWHM, limited by the photon lifetimes of $\sim$5-10 ps in the high-Q laser cavities. It was possible to obtain shorter delays and shorter output pulses by reducing the photon lifetime, resulting in higher laser thresholds as expected.

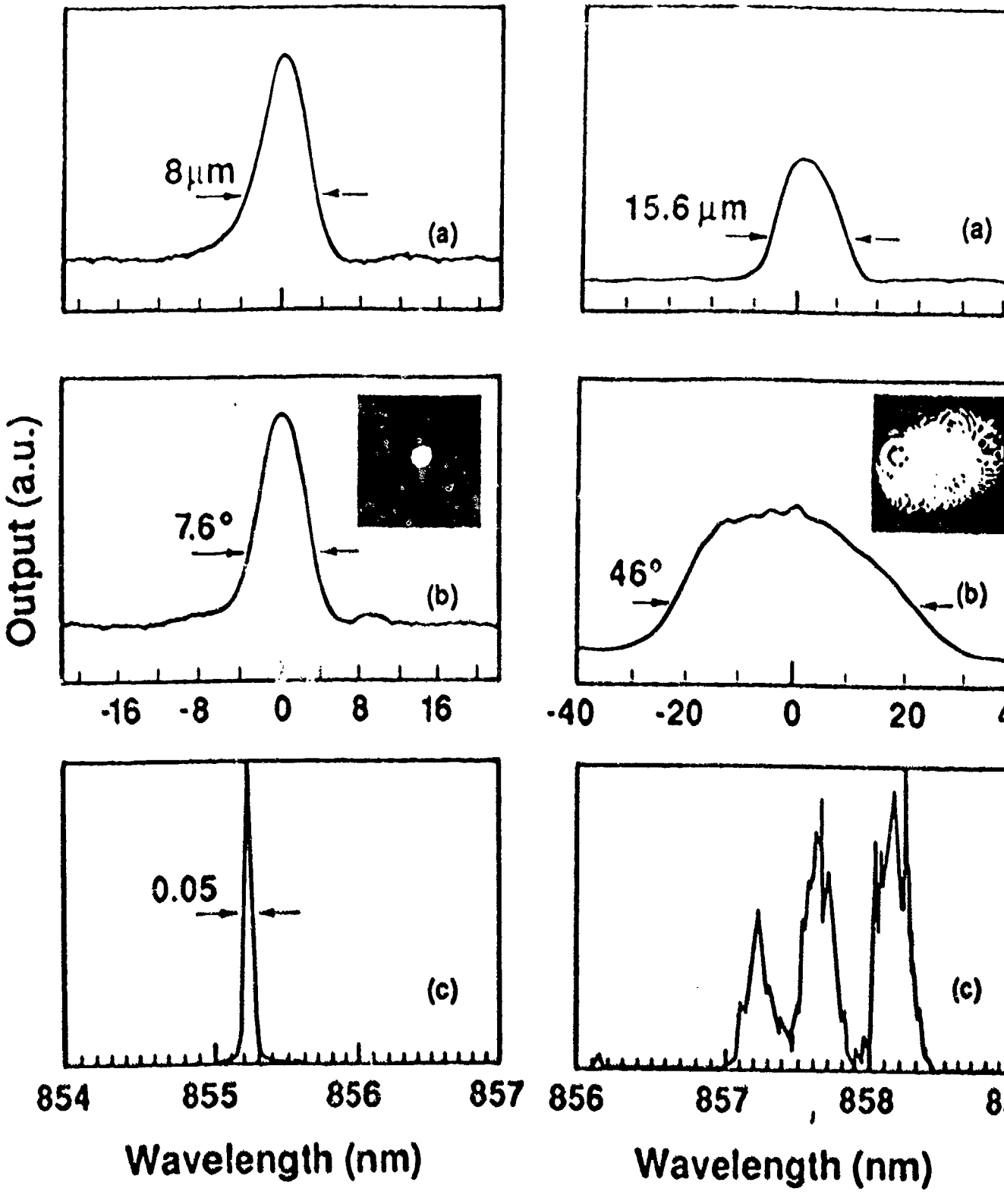


**FIGURE 7**

Near-fields, far-fields and optical spectra for a GaAs/AlGaAs RPG-VCSEL at (a) 2 mW and (b) 15 mW output power.

A rate equation model has been constructed to describe the dynamical properties of the optically pumped VCSEL. The rate equations for the carrier density $N(t)$ and the photon density $S(t)$ are

$$dN/dt = P - N/\tau_s - gS(N-N_{tr}) \quad (3)$$

and

$$dS/dt = -S/\tau_p + gS(N-N_{tr}), \quad (4)$$

where $P$ is the (optical) pumping rate per unit volume, $g$ the gain, $\tau_s$ and $\tau_p$ are the spontaneous carrier recombination time and photon lifetime respectively, and $N_{tr}$ the carrier density required to achieve transparency in the semiconductor. These equations were integrated numerically, and a typical set of results is shown in Figure 8: the pump pulse rapidly generates a carrier population which decays more slowly to generate the VCSEL output pulse whose width is limited by $\tau_p$. A switch-on delay of a few $\tau_p$ is also typical. The pulse shape calculated (without adjustable parameters) using this rate equation model compares exactly with that measured by cross-correlation with the input pulse, as is evident in Figure 9. A more detailed experimental and theoretical comparison of the VCSEL switching characteristics as functions of pump power is shown in Figure 10, again demonstrating excellent agreement. Here we see clearly that the pulse width saturates at about $2\tau_p$, the switch-on delay at about $5\tau_p$.

These experiments have demonstrated the feasibility of using VCSELs in high-speed optical switching roles. However, there are several interesting issues and problems which have surfaced: what is the temporal behavior of the transverse and longitudinal coherence length? why are the optical pumping efficiencies anomalously low using picosecond pulses (compared with CW efficiencies)? are the pulse spectra (*e.g.* the chirp) suitable for further compression or amplification? These issues will be addressed in our future research.

Because of the limited peak power and poor beam quality produced by the picosecond dye laser pump source at 740 nm - the dyes used at these wavelengths are relatively inefficient - we repeated the experiments using a newly-acquired mode-locked Ti:sapphire laser. This source generated tunable 1.2 ps pulses, at ~80 MHz repetition rate, with average power of >1 W from 720 to 850 nm.

## 2.5 Systems compatibility: temperature sensitivity

Our initial results have shown that the properties of the MOCVD-grown RPG VCSEL wafers are extremely non-uniform. This is not because the crystal growers were inept, but because the structure itself is extremely sensitive to small (a few percent) variations in dimensions and compositions. This sensitivity prompted us to study the performance of a RPG-VCSEL as a function of ambient temperature.

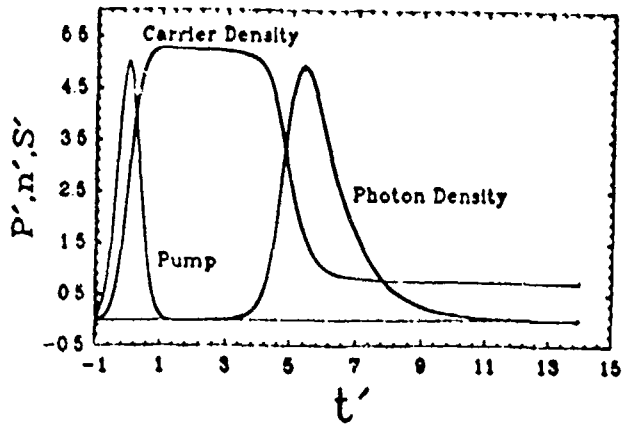


**FIGURE 8**

Rate equation based calculations of temporal evolutions of the carrier density and photon density (*i.e.* optical output power) in a RPG-VCSEL pumped by a picosecond optical pulse, also shown.

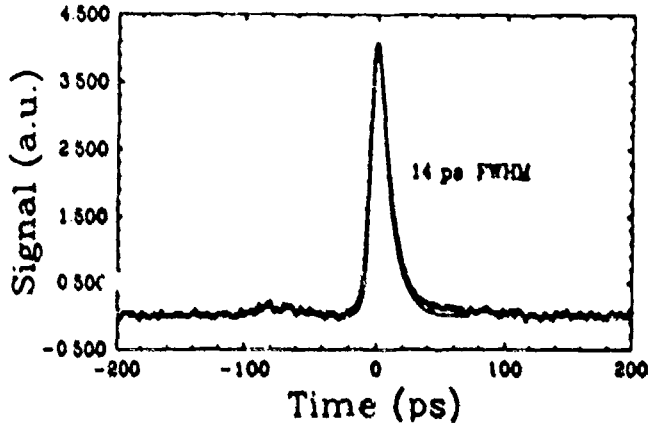


**FIGURE 9**

Comparison (by overlay) of pulse shapes experimentally measured (by cross-correlation with the pump pulse) and calculated based on the rate equation model with out adjustable parameters, showing excellent agreement.

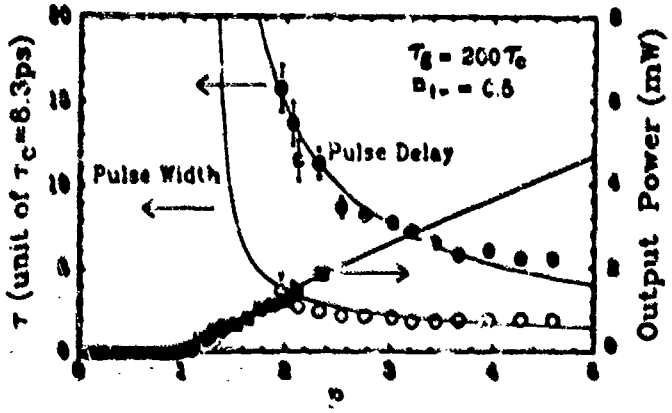


**FIGURE 10**

Comparison of calculated (solid lines) and measured (points) RPG-VCSEL output pulse width, switch-on delay and power, as functions of pump power, showing excellent agreement.

A GaAs/AlGaAs VCSEL with 20 quantum wells was optically pumped by a CW dye laser at 740 nm. The sample was mounted on a copper block whose temperature could be controlled to within 0.1 °C. A position on the wafer was chosen for its optimum performance at room temperature (300.5 K) and the laser mount temperature was then varied by 20 °C above and below the room ambient. Some of the results are shown in Figure 11, indicating significant changes in the threshold, quantum efficiency and spectral output with temperature changes as small as 5 °C. These preliminary experiments indicate the need for careful thermal design and ambient temperature control in practical applications. Optical switches designed around VCSELs should take this threshold variation into account, and wafer uniformity needs to be improved to $<1$ % for 2-D switch arrays operating above threshold. We note in passing that the nature of RPA switches which operate by saturation of the excitonic absorption (*cf.* Section 3 below) should make them inherently less sensitive to temperature and structural parameters than the VCSELs; consequently, it may be easier to fabricate uniform 2-D arrays of bistable RPA switches.

### 2.6 Power handling, scaling properties and large-area uniformity

It is anticipated that the above-threshold VCSEL-based optical switch may be used to handle large amounts of optical power in pulsed mode. We therefore conducted a series of experiments to determine the ability of the RPG-VCSEL to handle pulsed optical power. At first we wished to verify the conjecture that the RPG-VCSEL should permit the output power to scale with the emitting area because of suppression of lateral ASE. Hence we measured the threshold power per unit area for various spot sizes from 0.006 to 1 mm; in these measurements, the lower limit was established by lateral carrier diffusion, while the upper limit was imposed by the peak optical power available from the 7-ns, 10-Hz dye laser used to pump the VCSEL. Some of the data are shown in Figure 12, the flat curve of threshold power per unit area versus spot size indicating that the lateral ASE is being suppressed effectively by the RPG structure.

In a second series of experiments to determine whether the RPG-VCSEL switch could withstand high quasi-CW optical powers, a single-shot, flashlamp-pumped dye laser producing 500 ns pulses at 740-760 nm was used to pump GaAs/GaAlAs and InGaAs/AlGaAs RPG-VCSELs. The former structures lased up to 1 $cm^2$ diameter with peak outputs up to 20 kW, while the latter lased up to 0.1 $cm^2$ diameter with peak outputs up to 50 kW; at these high power levels, some of the wafers tested suffered catastrophic optical damage at the pump input surfaces.

## 3 OPTICAL SWITCHING IN RPA ETALONS

### 3.1 Bistable optical switching in a nonlinear etalon

Gibbs *et al.* have demonstrated bistable optical switching in a nonlinear etalon in which the optical nonlinearity is provided by multiple quantum wells [6]. In this research, we have sought to extend their design to reduce the

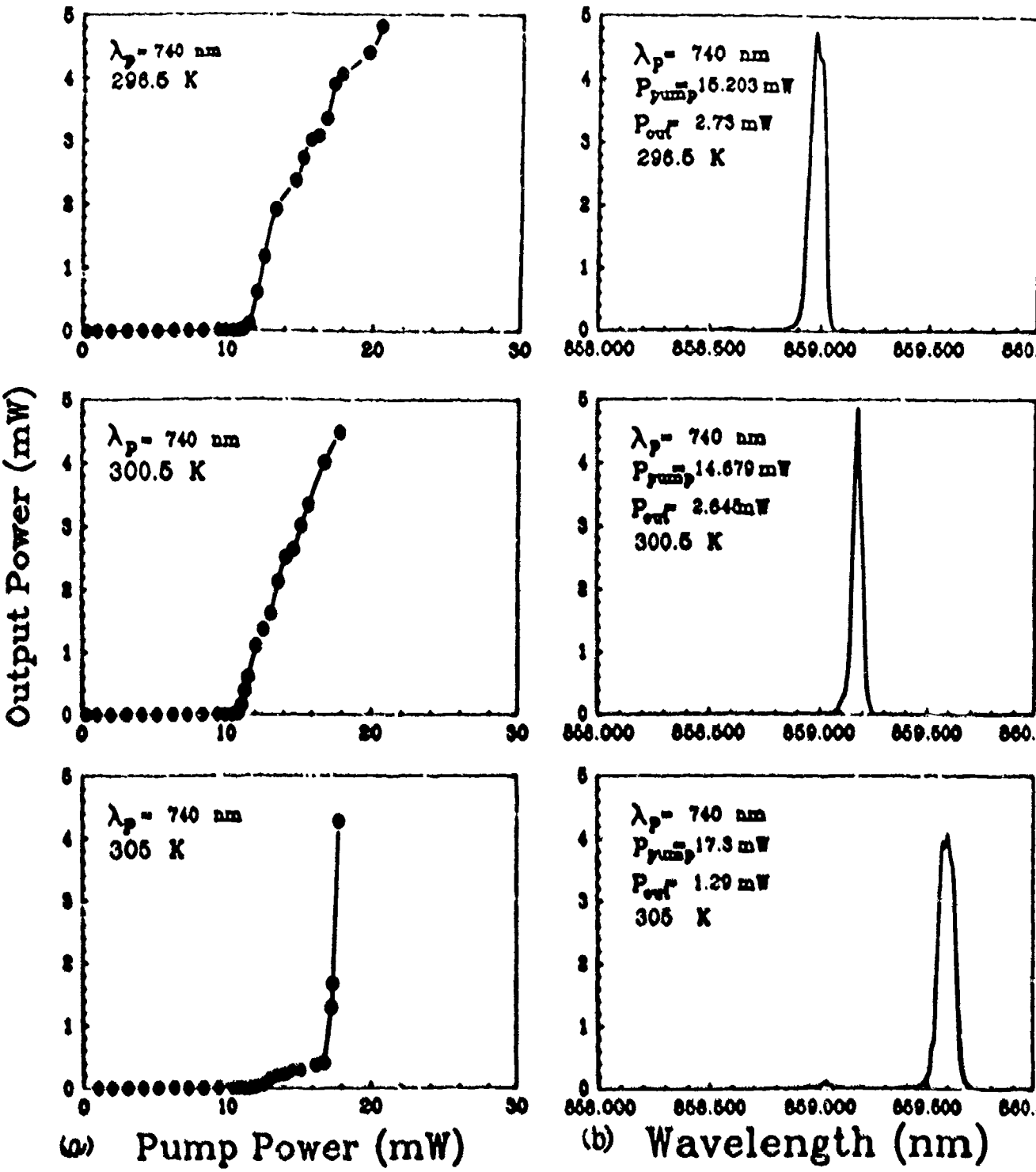


**FIGURE 11**

Experimentally measured input-output characteristics (a) and optical spectra (b) for a CW GaAs/AlGaAs RPG-VCSEL at three different ambient temperatures.

switching threshold, a particularly important issue if large-scale 2-D arrays of switches are to become feasible. Our general approach has been to design and build the switch wafers in a fashion analogous to development of RPG-VCSELs: first we space the quantum wells at half-wave intervals in order to maximize the overlap between the optical nonlinearity and the cavity standing wave, and second we will employ quarter-wave epitaxial multilayer reflectors for both mirrors of the etalon; this new RPA bistable etalon is illustrated in Figure 13.

### *3.1.1 Absorptive optical bistability*

Here we present a brief recapitulation of bistable optical switching. A bistable switch is a device which has two stable output states for a range of input states: it exhibits hysteresis in its input-output curve as shown in Figure 14, where the solid line represents the experimental performance of an ideal device and the dashed line represents a typical theoretical result. The performance of such a device may be evaluated on the basis of switching energy, switching range, contrast ratio and/or holding power. Such devices are essentially binary; there are no grey levels achievable, although optical multistability may be observed under certain conditions. As might be expected, optimization of any given performance parameter generally involves compromising on one or more other parameters. Figures of merit based upon some combination of the above parameters have been developed for comparing designs, but such comparisons generally presuppose a particular application and are subjective.

Optical bistability requires a nonlinearity and feedback. Bistability was first predicted in a system (a $CO_2$ laser with a $SF_6$ absorber cell) which depended on saturation of the absorption of some material placed within a Fabry-Perot etalon. This so-called absorptive optical bistability is still the simplest form of optical bistability conceptually, but it has never been observed without a strong dispersive component. In semiconductor-based systems such as diode lasers coupled to saturable absorbers, absorptive effects can be made to dominate.

Assume that we have a high finesse Fabry-Perot cavity which is filled with a saturable absorber. For simplicity the cavity is assumed to be exactly resonant at the wavelength of the incident light and the absorber is assumed to be totally saturable. If the incident intensity is $I_0$ then the intensity just before the output mirror is

$$I = I_0 T \exp(-\alpha L) \tag{5}$$

and the transmitted intensity is

$$I = I_0 T^2 \exp(-\alpha L) \tag{6}$$

where $\alpha$ is the absorption coefficient, $L$ is the cavity length and $T$ is the mirror transmission. Eq. (6) is valid if the saturation intensity $I_{sat}$ of the medium is large with respect to the intracavity intensity, *i.e.* if $I_{sat} > I_0 T$.

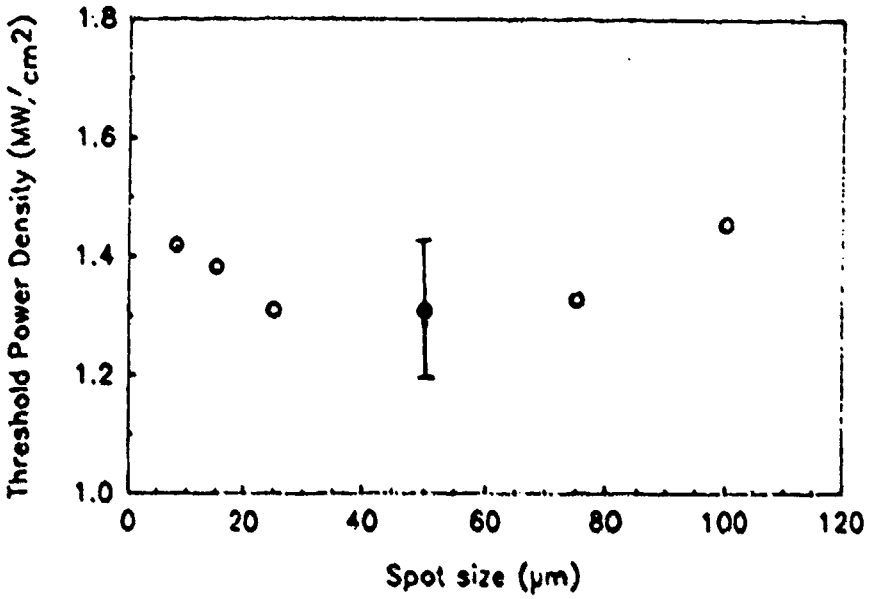


**FIGURE 12**

Measured threshold pump power per unit area for various spot diameters from 6 μm to 100 μm, showing a flat characteristic within experimental error.

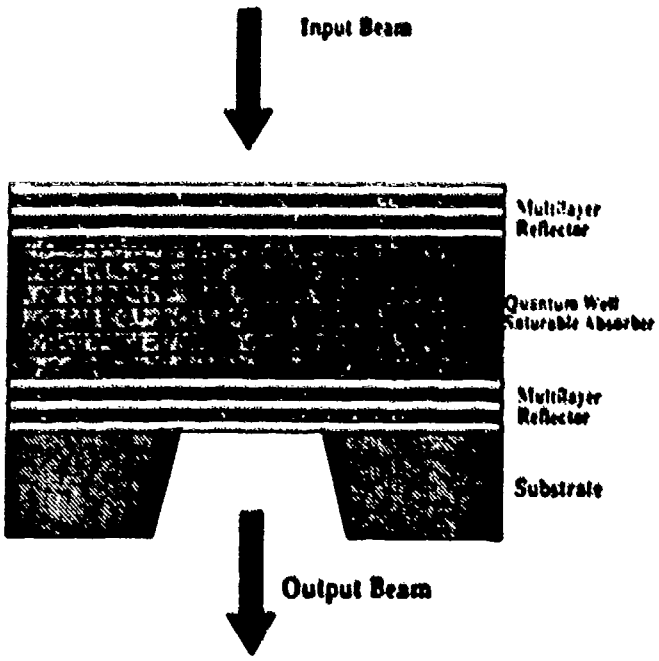


**FIGURE 13**

Schematic diagram of absorptive bistable switch based on transmission through an RPA medium inside a high-Q etalon.

**FIGURE 14**

Schematic of the input-output power hysteresis loop characteristic of bistable optical devices.

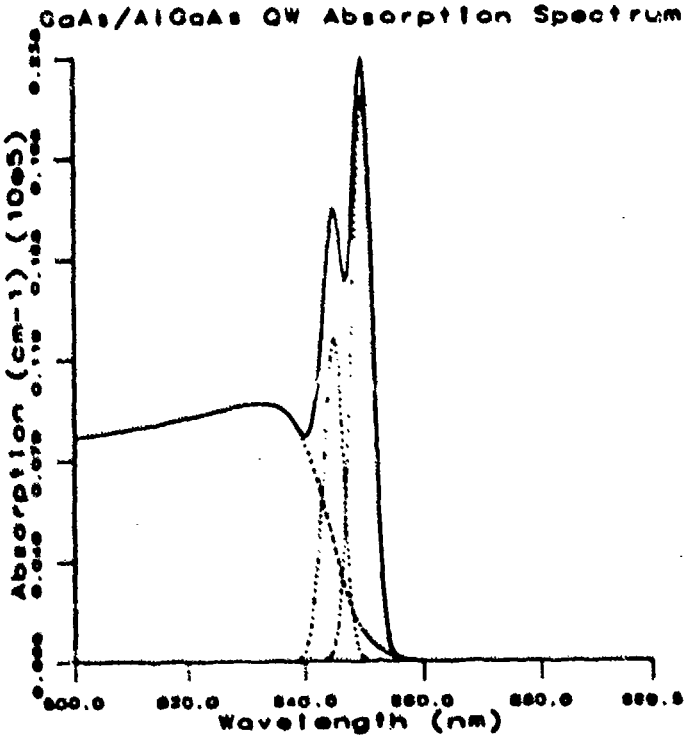


**FIGURE 16**

Semi-empirical approximation to the quantum well optical absorption spectrum: light- and heavy-hole excitons give saturable Gaussian features superimposed on an unsaturable band-to-band continuum.

Figure 15(a) is a schematic representation of the optical intensity in the system when the absorption is unsaturated. At some value of the input intensity, $I_{sw}$, the absorption saturates and the internal cavity intensity increases dramatically. A rapid switch-up is seen in the output at this point. We then have a high finesse cavity where the output intensity is almost the same as the input intensity and the internal intensity is many times the input intensity: $I_t \sim I_0$ and $I_{in} \sim I_t/T$. This clearly holds for $I_{in} >> I_{sat}$, *i.e.* if $I_0 > TI_{sat}$. This situation is depicted in Figure 15(b). After the saturation intensity is reached, the system output will once again increase linearly with input, with a relatively high transmission factor.

If we now begin to decrease the input intensity, we see that due to the cavity finesse we may reduce the input beyond $I_{sw}$ before the intra-cavity intensity falls enough for the absorber material to again absorb. This situation is represented in Figure 15(c). When $I_{in}$ does fall below the saturation value, $I_{sat}$, a rapid switch-down will occur. We may see the possibility of bistability by noting that Eqs. (5) and (6) may both be satisfied by the same value of $I_0$ over a finite range of input intensities.

### *3.1.2 Absorptive* vs. *dispersive bistability in nonlinear etalons*

Optical bistability was first observed experimentally by Gibbs *et al.* in a sodium vapor filled etalon [7]. Upon examination, however, the data did not quite match the predictions generated by an absorptive model. Examination of this discrepancy led to the realization that dispersive bistability occurs in addition (and often in preference) to absorptive bistability in atomic systems.

Dispersive bistability occurs in a nonlinear medium with an intensity-dependent index. The etalon is designed to be off-resonance initially, but tunes into resonance with increasing intensity. As in the absorptive case, once the cavity is on resonance the high finesse results in the intracavity field remaining quite high as the incident power is reduced. This results in a memory effect, and hence hysteresis. In practice, due to unavoidable coupling between the real and imaginary parts of the refractive indices of real materials, both absorptive and dispersive effects contribute to the switching in realizable devices. In some cases, dispersive effects have been shown to dominate and accurate predictions may be made by neglecting absorptive effects. Our initial theoretical investigations have been for a purely absorptive nonlinearity. This is because suitable data is not available for the coupling between the real and imaginary components of the refractive index of quantum well materials over the intensity range we require. We plan to perform the necessary measurements on a MQW calibration sample to allow us to incorporate dispersion in the model as it is unlikely that an optimal design can be developed without accounting for dispersion. We may however, demonstrate the first instance of absorption-dominated bistability as our design enhances absorptive interaction while having the same dispersive contribution as previous MQW devices.

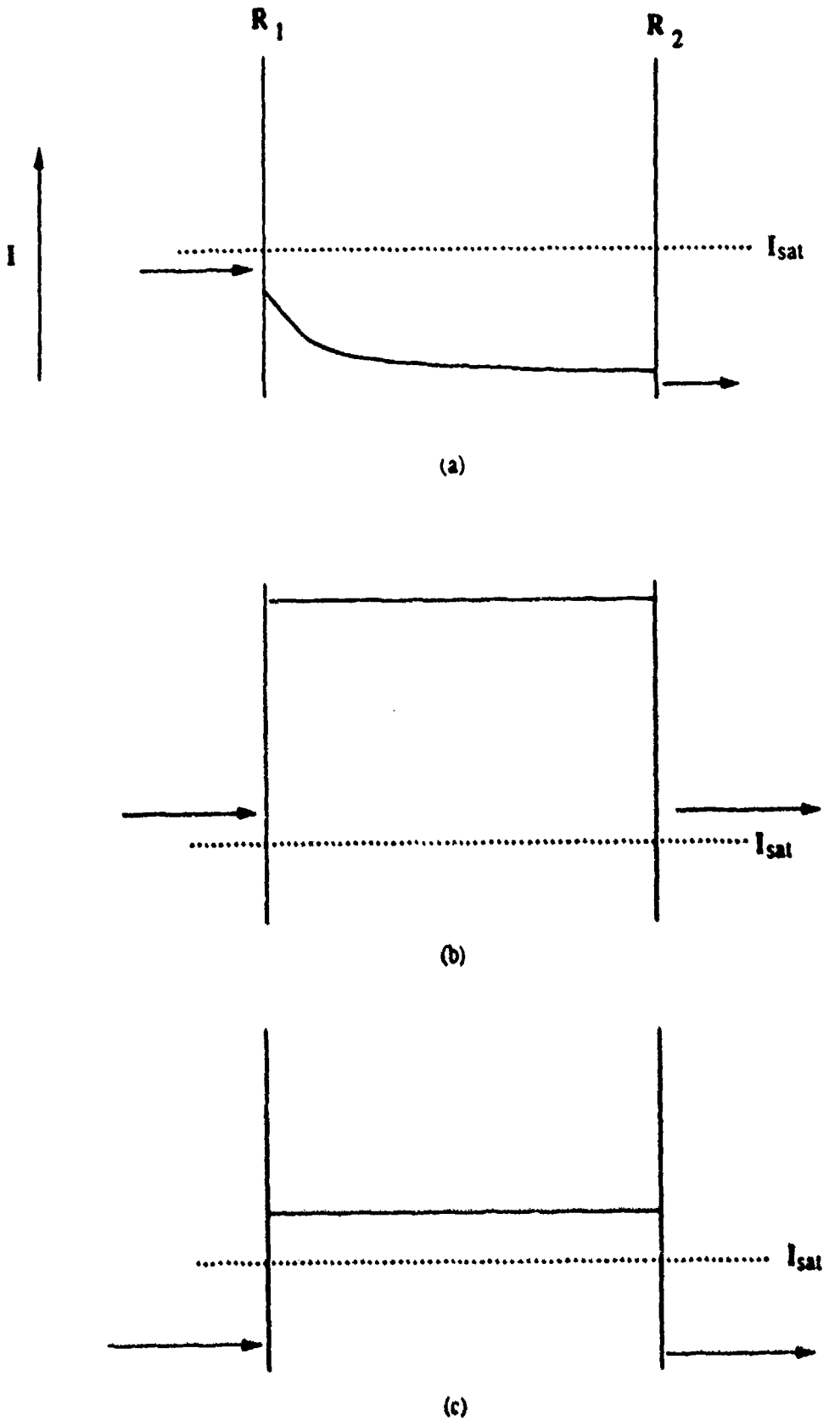


**FIGURE 15**

Schematic of axial intensity distribution in an absorptive bistable optical switch at various input intensities relative to the saturation intensity $I_{sat}$.

The saturable absorption feature used in our design is the heavy-hole excitonic resonance. It is well known that the excitonic resonances in quantum wells are enhanced by the increased Coulombic attraction caused by the quantum confinement [8]. It is also known that these resonances are easily saturated [9]. The saturation may be understood as a coulombic screening by the free carriers within the wells. Excitons which are formed by absorption of photons just below the band gap are thermalized almost immediately and become conduction band electrons. These electrons then screen the electron-hole attractions, preventing further excitonic absorption. This saturation effect is enhanced by the quantum confinement.

Excitonic absorption saturation is a prime mechanism for bistable optical switching: on resonance, the saturation intensity should be low (a few hundred watts per square centimeter) and the unsaturable losses should be small, leading to high on/off contrast and low insertion loss, as well as ready extension to 2-D arrays.

## 3.2 Theoretical modeling of RPA bistable switches

### *3.2.1 Representation of the quantum well absorption:*

For our calculations, we have used the phenomenological curve fit developed by Miller and Chemla to describe the low intensity (unsaturated) absorption of a quantum well system [8]. They found that the absorption is well described by Gaussian features for the light- and heavy-hole excitons plus a broadened 2-D continuum for the band edge, as shown in Figure 16 and expressed by the relation

$$\alpha(\omega) = \alpha_h Exp\left[-\frac{(\omega - \Omega_h)^2}{2\Gamma_h^2}\right] + \alpha_l Exp\left[-\frac{(\omega - \Omega_l)^2}{2\Gamma_l^2}\right] + \left[\frac{\alpha_c}{1 + Exp\left[\frac{(\Omega_c - \omega)}{\Gamma_c}\right]}\right]\left[\frac{2}{1 + Exp\left[-(\hbar\Omega_c - \omega)/R_y\right]^{1/2}}\right] \quad (7)$$

where $R_y = e^2\mu^*/8\pi^2\epsilon^2\hbar^2$ is the exciton Rydberg constant with $\mu^*$ the effective mass of the electron-hole pair, $\epsilon$ the permittivity, the $\Omega$s and $\Gamma$s are the resonant frequencies and damping constants for the heavy holes ($h$), light holes ($l$) and the band-to-band continuum ($c$, no $\Gamma$). We have used this expression with constants determined experimentally, with the excitonic features saturating as

$$\alpha = \alpha_0/(1 + I/I_{sat}), \quad (8)$$

while the band-to-band continuum is assumed to be unsaturable. This assumption is adequate as the state-filling saturation of the continuum requires at least two orders of magnitude higher intensity than the Coulombic

screening saturation of the excitons. Values for $I_{sat}$ in the literature vary widely; a recent reliable study by Lee *et al.* [9] reported 250 W cm$^{-2}$, and we have used a conservative 300 W cm$^{-2}$ in our calculations.

### 3.2.2 *Modeling the bistable switch*

To calculate the switch transfer function, we use the thin-film matrix formalism commonly applied to multilayer interference filters. By this method the left and right-going electric fields at the left of a dielectric stack (or part of a stack) may be expressed in terms of the known field to the right. We may then step through a range of output intensities and calculate the corresponding input intensities thereby producing an input-output curve. The model as written is one-dimensional and consequently neglects diffusion, diffraction and beam intensity distributions.

The code written to date has been intended only to compare the performance of nonresonant and resonant quantum well switches and not to design switches. For simplicity, we have modeled the devices as having single reflecting layers rather than multilayer reflectors. Figure 17 illustrates the switches as modelled: a stack is generated in which the real parts of the refractive index of all layers are constant. We begin with an assumed output intensity, convert that to a right-going electric field and compute the field at the right of the first (from the right) quantum well. At this point we compute the absorption in that well using Eqs. (7) and (8) and determine the real part of the index within that well. Using this index, we find the intensity at the right of the next well and so on through the entire structure.

### 3.2.3 *Saturable* vs. *unsaturable losses*

Because unsaturated losses (background absorption and scattering) reduce the contrast ratio, the switch was designed to operate at the wavelength offering the highest ratio of saturable to unsaturable absorption. Figure 18 is a plot of this ratio based on the absorption model outlined in Sec. 3.2.1. Comparing this to the curve of low intensity absorption, it may be seen that the greatest value of this ratio occurs just slightly below the heavy-hole exciton center energy. All subsequent calculations were performed at this wavelength (850.5 nm).

### 3.2.4 *Resonant* vs. *non-resonant MQW absorber structures*

To evaluate the effect of our design "improvements", we attempted to compare resonant-well and nonresonant-well switch designs. This is not a straightforward exercise, however, because etalon resonance was not achieved for structures where the sum of the optical path lengths of one spacer and one well was a half wavelength. Plots of the Fabry-Perot transmission spectra of such a switch (without absorption) reveal that there is a shift of the transmission modes around the design wavelength (Figure 19) arising from out-of-phase reflections from the different interfaces within the structure. It is therefore necessary to iteratively design the spacer thicknesses so

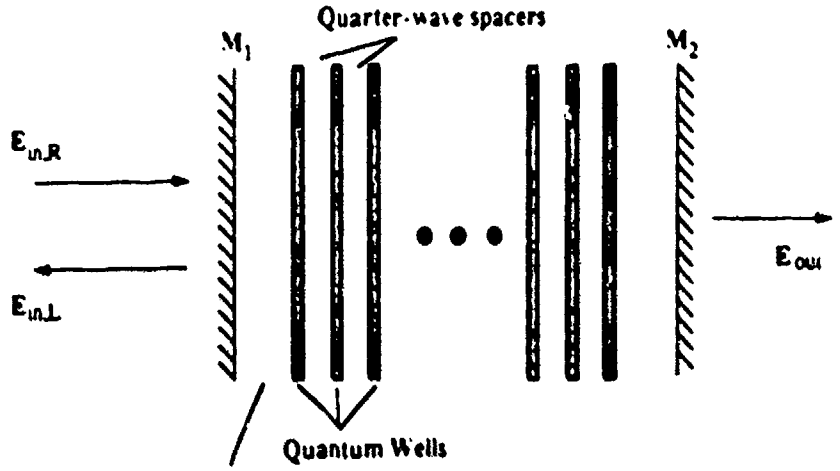


**FIGURE 17**

Schematic of RPA bistable optical switch design parameters.

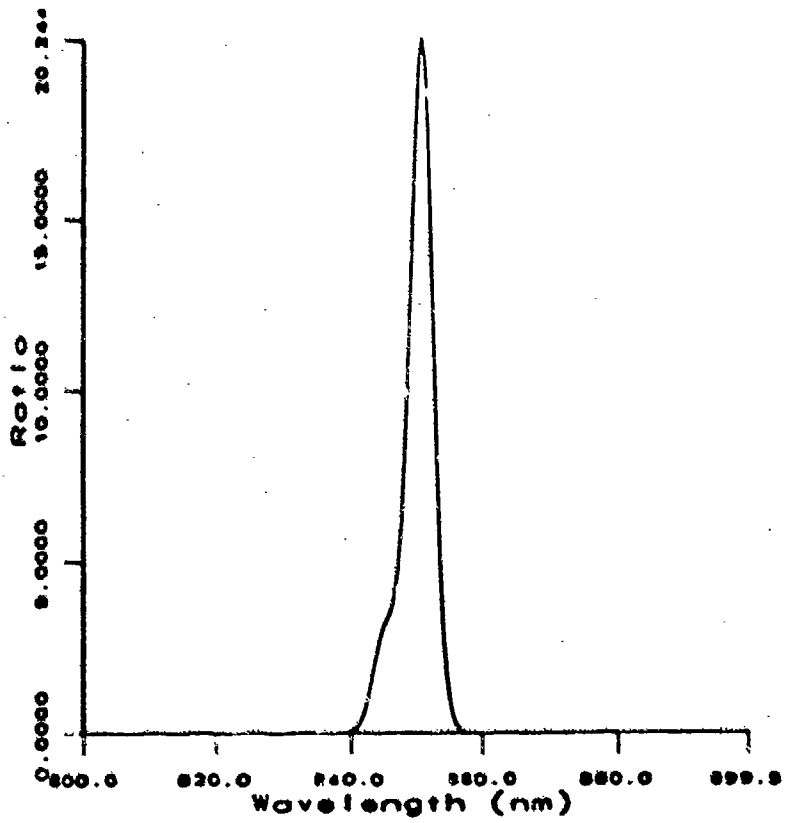


**FIGURE 18**

Spectral dependence of the ratio of saturable to unsaturable absorption, calculated based on the semi-empirical total absorption spectrum given in Fig. 16, showing a narrow peak at 850.5 nm.

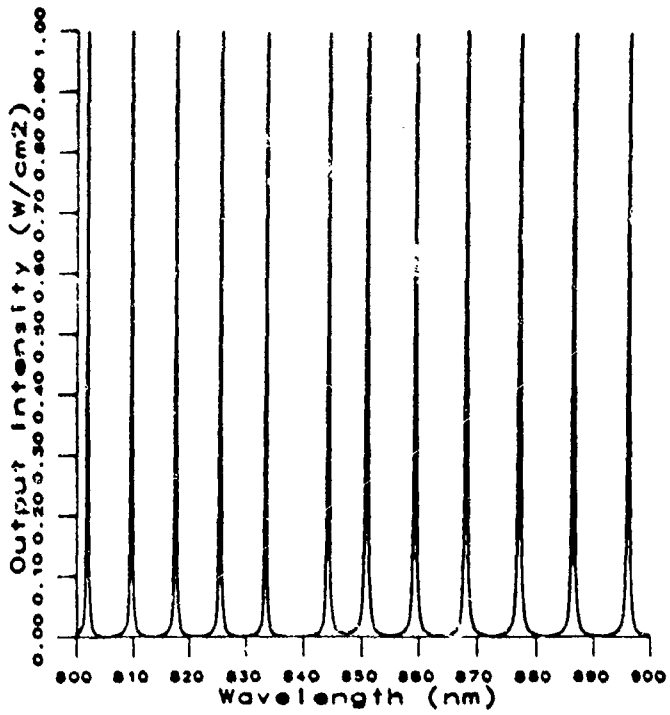


**FIGURE 19**

Calculated Fabry-Perot spectra for the structure in Fig. 17.

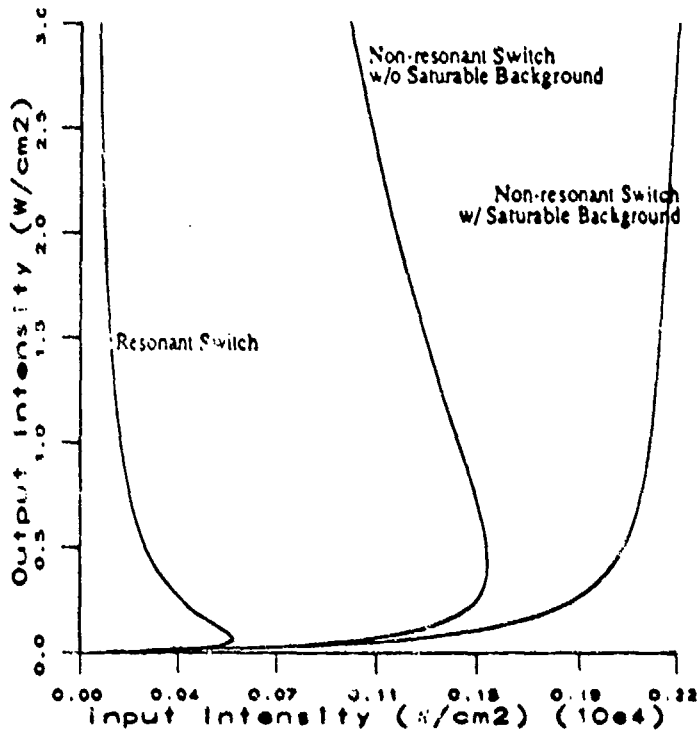


**FIGURE 20**

Calculated intensity transfer functions for resonant (RPA) and non-resonant 100-well structures within high-Q etalons. The non-resonant structure is bistable only when the unsaturable background is neglected - an unrealistic requirement - and even then with a switching threshold a factor of three or so higher than that of the RPA structure, which is tolerant of the unsaturable absorption.

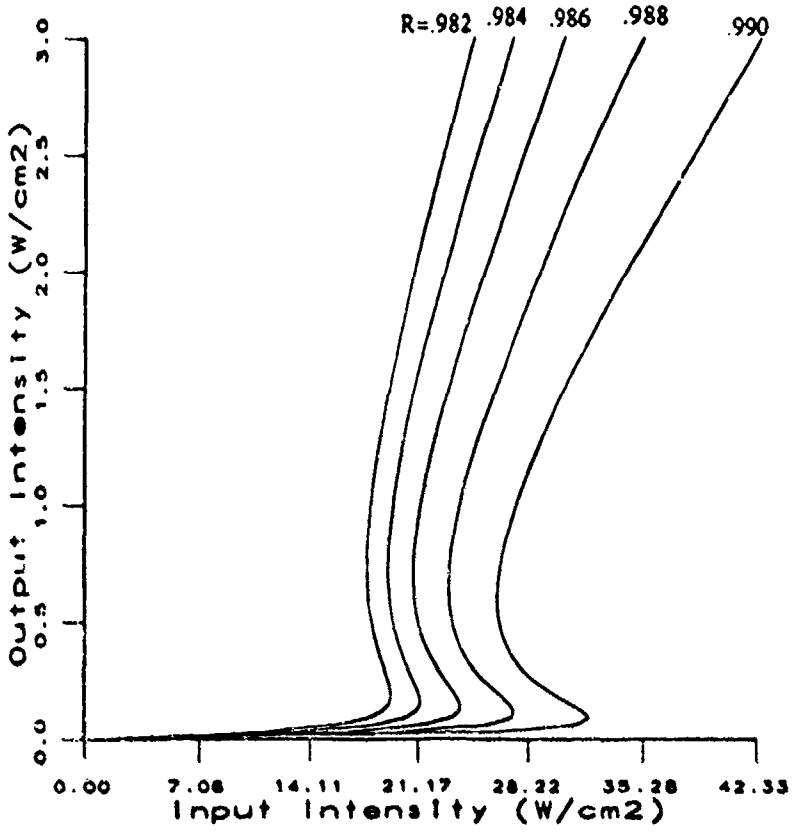


**FIGURE 21**

Calculated intensity transfer functions for 20-well RPA etalons for various reflectivities from $R = 0.980$ to 0.998

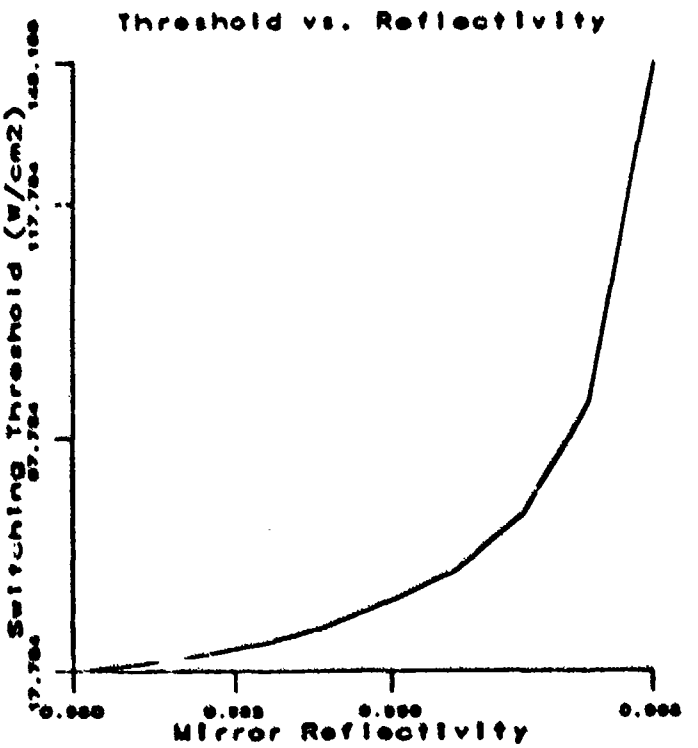


**FIGURE 22**

Calculated switching threshold vs. reflectivity in the same range as Fig. 21.

that the etalon resonance will occur at the design wavelength (850.5 nm in this case). The high reflectivities we are likely to need (>95%) result in narrow Fabry-Perot transmission features which make this matching critical.

With this procedure, we have calculated the transfer functions of various resonant and non-resonant switch designs. It was seen that bistable operation for a non-resonant structure requires 100 quantum wells with the constants used in our calculations, even with the unsaturable continuum absorption set to zero. Figure 20 shows the transfer functions of 100-well structures for the resonant and non-resonant cases, where the non-resonant well results are shown both with and without an unsaturable background. We see that a reduction in the switching threshold improvement by a factor of four may be achieved by resonant half-wave spacing of the saturable absorption sheets.

### *3.2.5 Optimization of switching threshold and on/off contrast*

Next we investigated the tradeoff between switching threshold and bistable switching range offered by different mirror reflectivities. This is another potential improvement of our switch design, as we are able to control the end mirror reflectivities very accurately in our epitaxial multilayer reflectors. Figures 21 and 22 show switch transfer functions and thresholds of a 20-well RPA switch for several different end reflectivities, indicating that a switching threshold of less than 20 W/cm$^2$ is possible with very high reflectivities, but at a large sacrifice in the bistable range. Our calculations suggest using a compromise value of 99% for the mirror reflectivities, to provide a reasonably low threshold (32 W cm$^{-2}$) and usable switching range (about 6 W cm$^{-2}$). When reflectivities lower than 99% are used, the threshold increases rapidly after this point.

## 3.2 Absorption spectroscopy of VCSEL wafers for RPA switching

For our initial experimental work, we used vertical-cavity surface-emitting laser samples configured for low-threshold CW optical pumping and performed absorption spectroscopy to determine the locations of the light- and heavy-hole excitonic resonances. These data are to be used in the second-generation theoretical model, especially for designing the custom RPA bistable switch wafer.

Two MOCVD-grown GaAs/GaAlAs resonant periodic gain multiple quantum well (RPG-MQW) samples with 20 half-wave-spaced quantum wells and epitaxial multilayer high-reflectivity stacks with $R$=0.995 and 0.999 were placed in the experimental arrangements depicted in Figure 23. A white-light source illuminated each sample, and the transmitted and reflected light was measured using an optical multichannel analyzer (OMA). From these measurements the optical absorption of each sample was deduced. Despite some residual Fabry-Perot fringes (caused by imperfect subtraction of the reflection and transmission patterns) there were clear excitonic resonances at 851.3 and 846.0 nm (see Figure 24). The former resonance, due to the heavy-hole exciton, is the intended

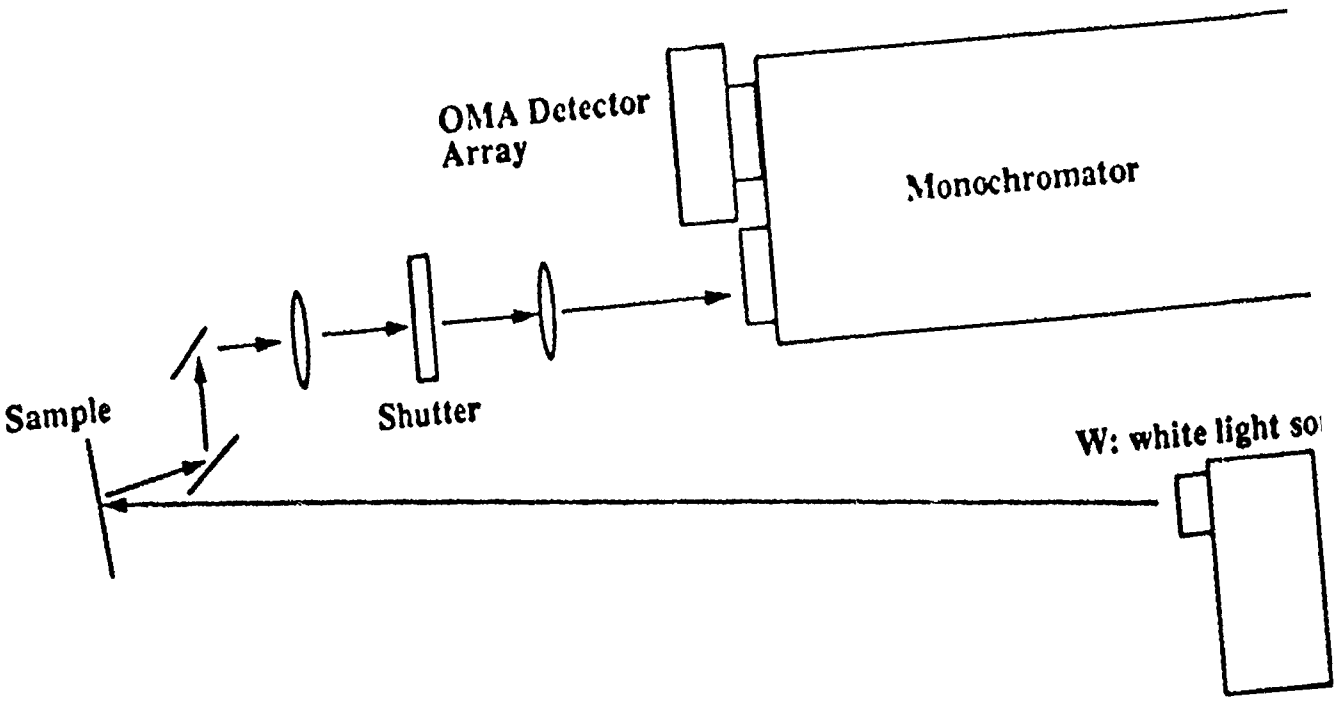


FIGURE 23

Experimental arrangement used to measure the reflection and transmission spectra $R(\lambda)$ and $T(\lambda)$ of a RPA sample without end reflectors; the absorption spectrum was then determined as $1\text{-}R(\lambda)\text{-}T(\lambda)$.

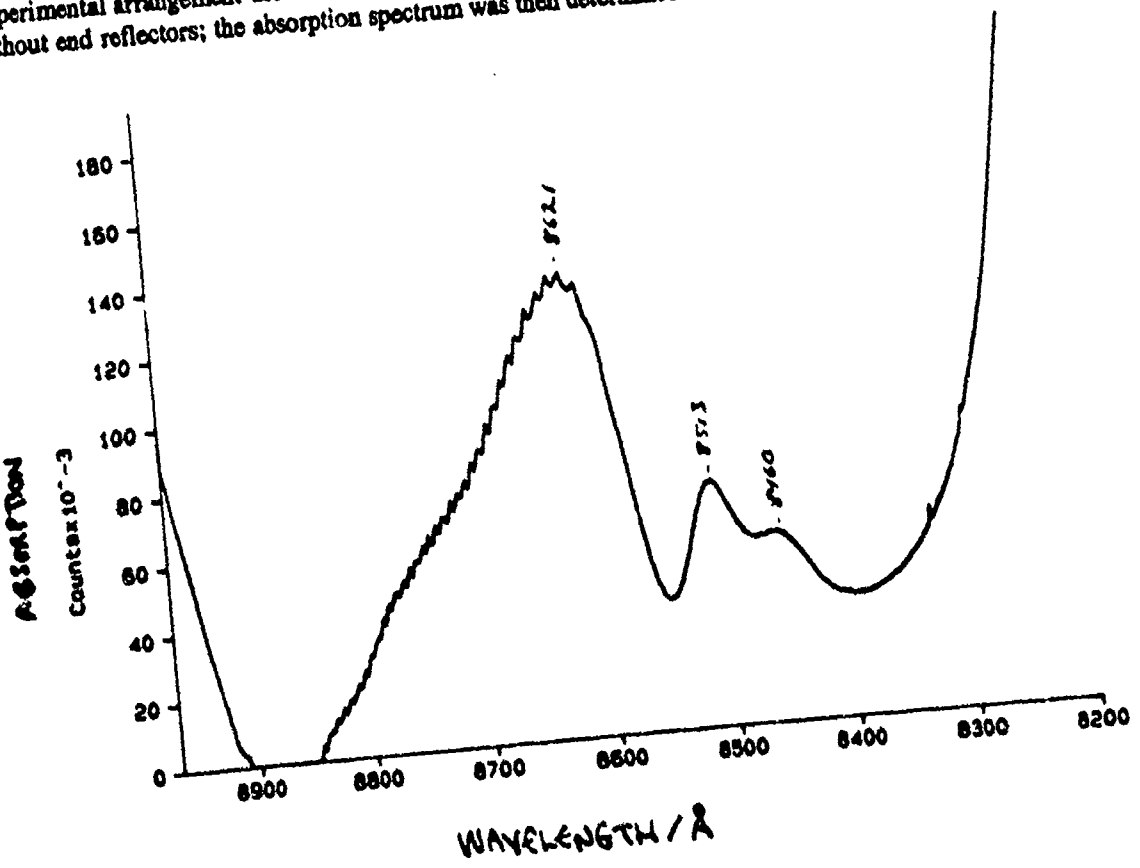


FIGURE 24

Absorption spectrum determined as described in Fig. 21, showing the excitonic features. These data will be used to design custom wafers for RPA switching.

basis for our optical switch. This information will therefore allow us to design a specific high-Q cavity structure with a transmissive mode close to this wavelength.

Further experimental tests were performed on these wafers, to determine whether absorption saturation at ~300 W cm$^{-2}$ could be observed, using the arrangement illustrated in Figure 25. The beam from a mode-locked Ti:sapphire laser was directed onto an acousto-optic modulator for precise frequency shifting, then shone onto the RPA sample, whose transmission was measured as functions of incident power and wavelength. Based on the reflectivity spectra and our initial calculations, we concentrated on the wavelength region from 845 to 960 nm, the range of input powers being 0.92 to 62.5 mW; for the 2 mm collimated beam used, and allowing for the use of 1.8 ps pulses at 80 MHz repetition rate, the latter figures represented peak intensities of ~50 to 3000 W cm$^{-2}$.

Unfortunately, the wafers used were optimized for operation as RPG-VCSELs, and no indication of absorption saturation was observed. This result is being examined closely, because the sample transmission was ~0.20, which suggests that saturation may already have taken place, although we had expected $I_{sat}$ to be in the range 250-1000 W cm$^{-2}$. Our next immediate steps are (1) to repeat some of the experiments at lower powers using more sensitive diagnostics, and (2) to procure and test a custom-grown wafer (according to the design described in Sec. 4 below) optimized for absorptive bistable switching.

As reported previously, a semi-empirical model due to Chemla *et al.* [8] has been used to design our switches. We had hoped, following the work of Lee *et al.* [9], that these experiments would enable determination of all the parameters of that model, particularly the saturation intensity $I_{sat}$. Although we have determined the exciton resonance wavelengths (essential for designing the sample and the next set of experiments) the data were not suitable for accurate determination of $I_{sat}$. In fact, we are re-thinking whether to re-cast the theory in terms of a saturation carrier density $N_{sat}$. This would be a more meaningful paramater but would be less accessible to direct measurement.

## 4 DESIGN OF IMPROVED BISTABLE SWITCH WAFERS

Using the semi-empirical model of Chemla *et al.* together with parameters we have measured experimentally and our matrix-propagation model for multilayer absorptive structures, we have designed a multiple quantum well GaAs/AlGaAs vertical-cavity bistable switch wafer. The resulting reflectivity spectrum, with a dip at the target wavelength of 851.3 nm, is shown in Figure 26.

In the next phase of our experimental work, and following some further optical pumping experiments using a tunable Ti:sapphire laser, this design will be used to fabricate a bistable switch wafer for final testing.

**FIGURE 25**

**Experimental arrangement used to test for absorption saturation in RPA structure without end reflectors; no measurable effect was seen.**

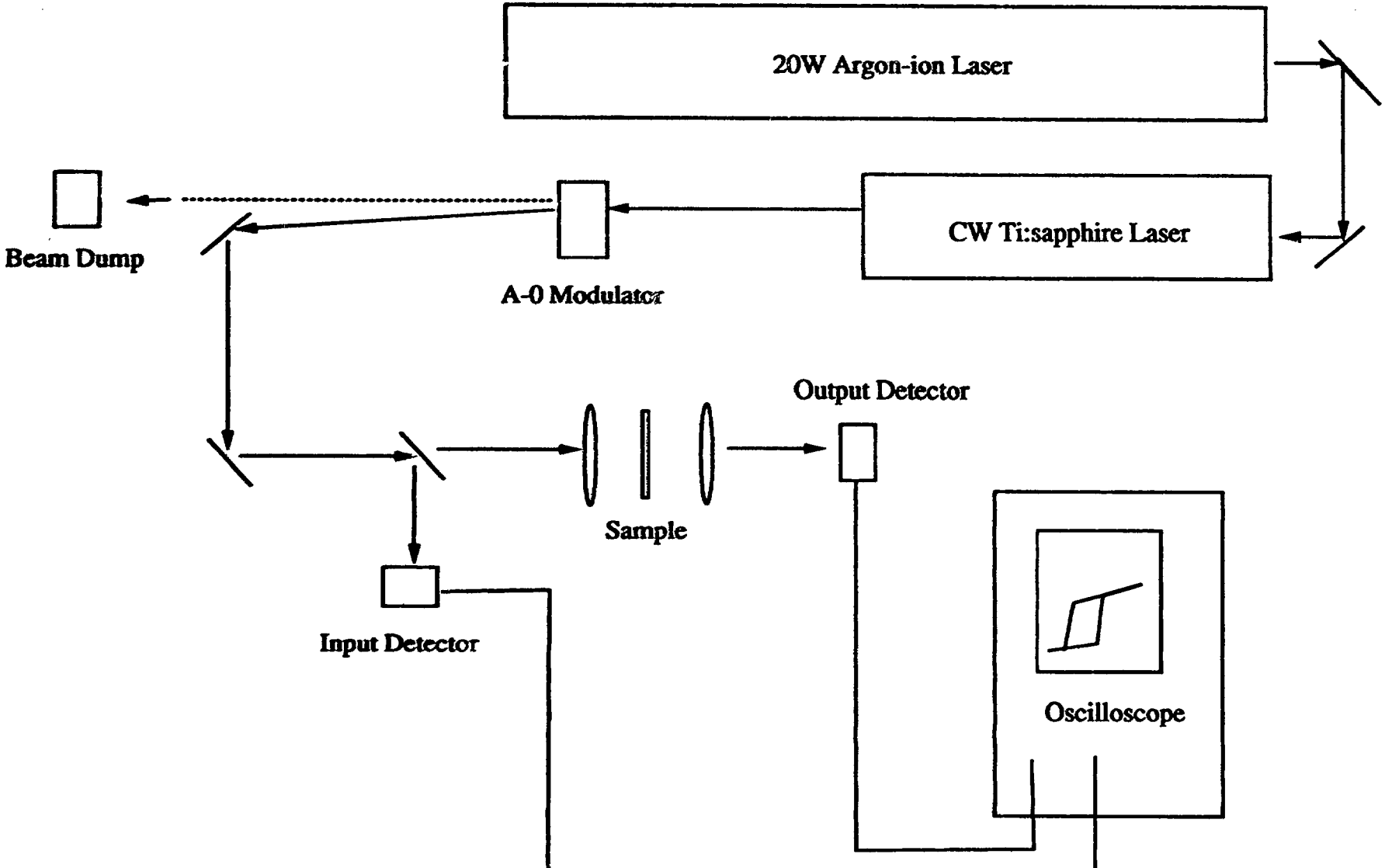

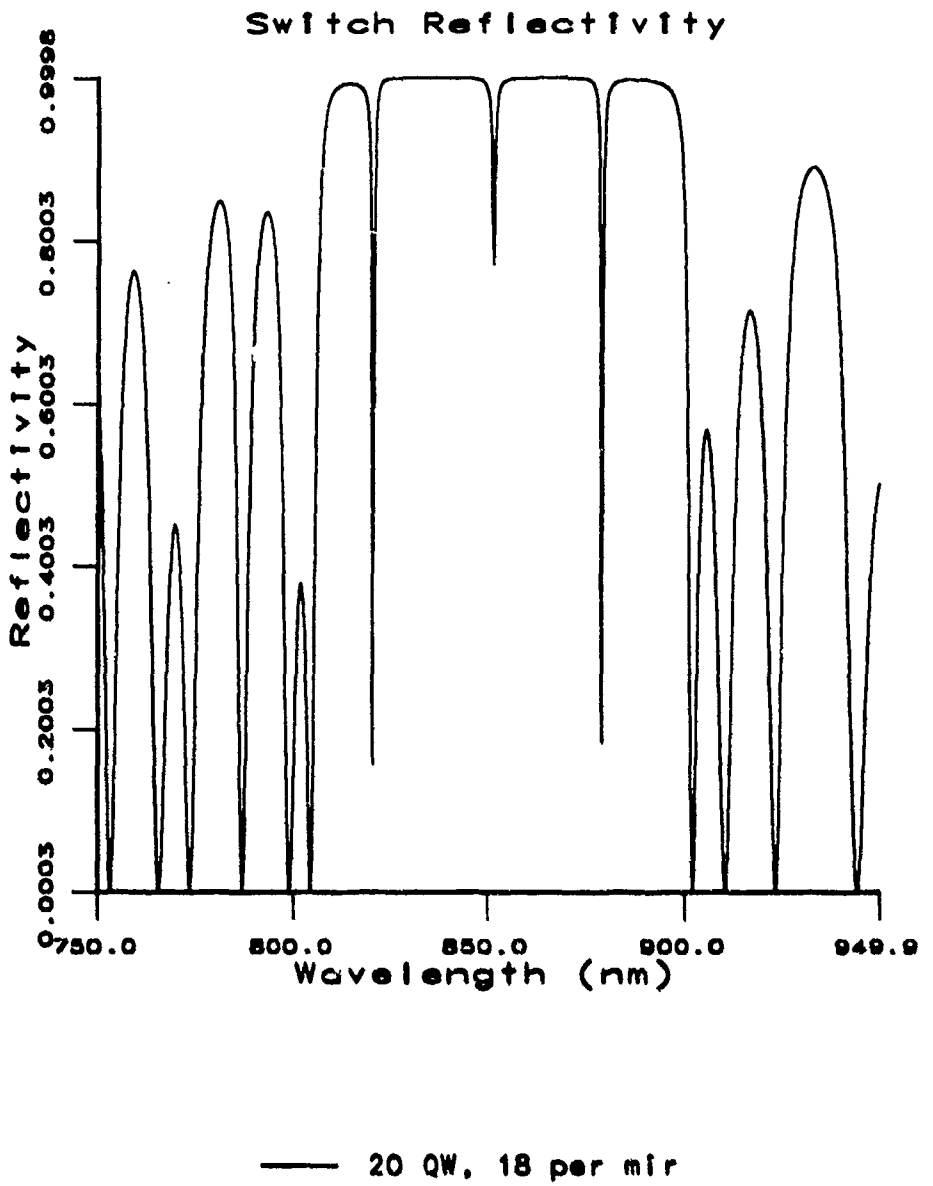


**FIGURE 26**

Calculated reflectivity spectrum for custom wafer design destined for RPA switch experiments; note the mode dip at 851.3 nm.

# 5 FUTURE DIRECTIONS

## 5.1 Extension to 2-D VCSEL arrays

Near the conclusion of this two-year project, we have demonstrated fast single-channel switching in above-threshold RPG-VCSELs; these can readily be extended into two-dimensional arrays. For greatest utility and versatility, these arrays (and hence the initial epitaxial wafers) should be as uniform as possible. Our initial experimental results and calculations indicate that compositions and dimensions should be controlled to within 1% or less. This is a factor of two or more better than the current state-of-the-art for metal-organic vapor phase epitaxy (MOCVD or MOVPE), and close to the best possible results using molecular beam epitaxy (MBE). The crystal growers have been persuaded of the importance of this work, and several substrate rotation arrangements and *in-situ* real-time growth diagnostics are being developed for MOCVD reactors, including the two at CHTM.

From a device physics point of view, we need to recognize that coherent optical power, even from an edge-emitting laser diode, is usually much more valuable and expensive than electrical power, especially when only low voltages ($<10$ V) and medium currents ($\sim 1$ A) are required. Consequently, we would like to design our next generation of active semiconductor laser-based switches as hybrids, biased electrically close to threshold for best efficiency, and triggered by optical pulses for highest speed. For extension to 2-D switching/modulation arrays, any non-uniformities in the materials, which result primarily in large threshold variations, can be offset partially by adjusting the currents to the various elements so that all are just below threshold. The optical power requirements for switching and the above-threshold switching performances of the various array elements should then be comparable even in the presence of large non-uniformities in the grown and processed structures.

## 5.2 Experimental verification of absorptive bistable switching in RPA etalons

Clearly the experiments intended to demonstrate bistable optical switching in RPA media inside high-Q etalons have fallen well behind schedule, mostly due to logistical problems such as crystal growth and access to suitable optical sources. The first set of such experiments will be completed early in 1992, by which time we hope to have a second-generation RPA switch wafer available for further experimental testing. Because of the low thresholds expected from RPA etalons, we do not anticipate major difficulties in extending the concept to 2-D switching arrays: the optical switching power and heat sinking requirements should be quite modest. The sample uniformity problems will still be vexing, and ultimately wafers with better than 1% uniformity in the optical thickness will be required.

As a companion set of experiments to the above, we will examine the interplay between absorption and dispersion in the RPA medium: this is a complicated question, and cannot be treated by a simple proportionality as in the

**FIGURE 27**

**Experimental arrangement to be used for transverse mode dynamical measurements in RPG-VCSELs.**

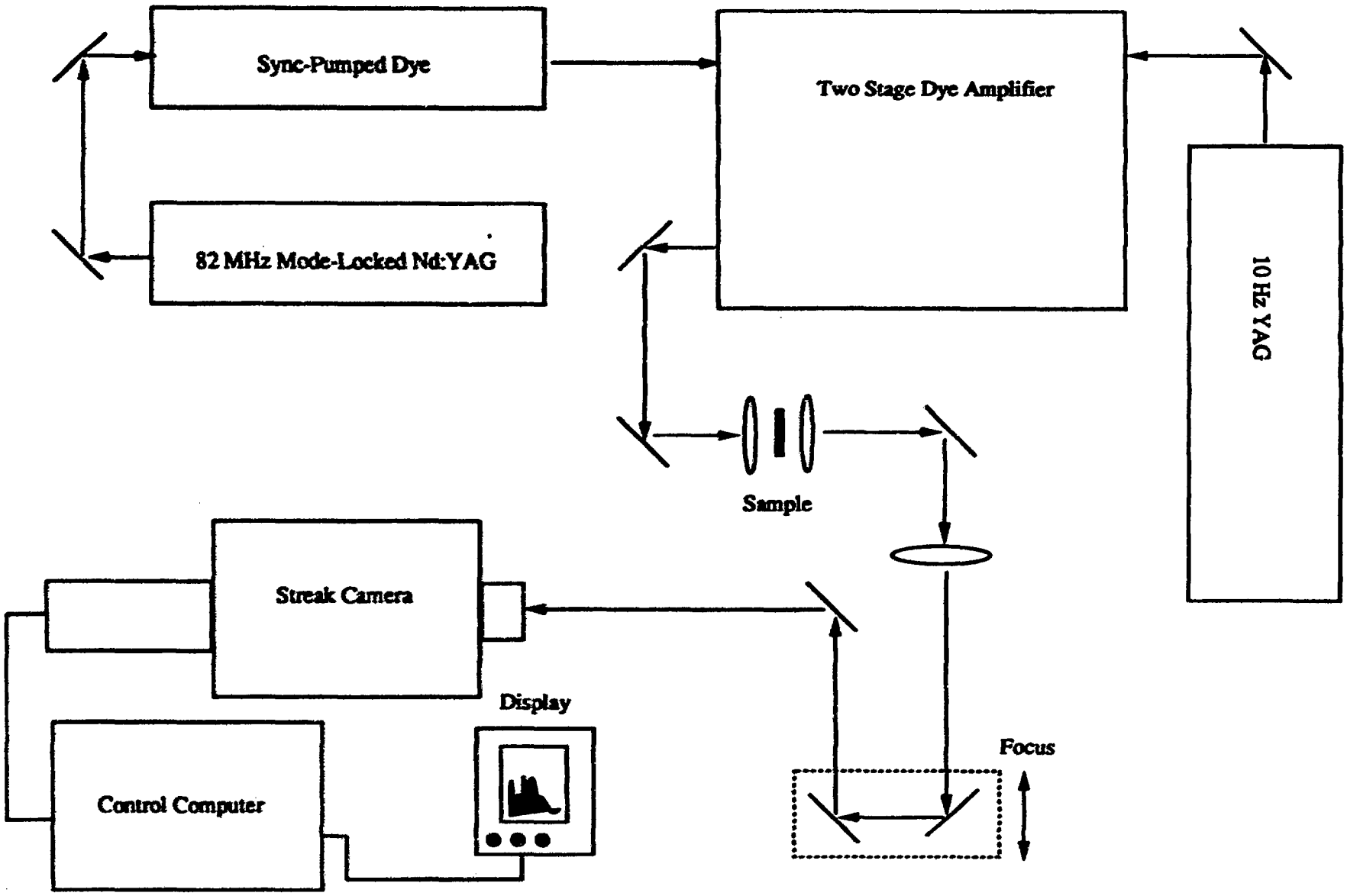

laser above threshold. A suitable experimental arrangement would be to place the RPA sample inside one arm of a Mach-Zehnder interferometer, allowing simultaneous measurement of the absorption and index change.

### 5.3 How can we achieve faster low-threshold switching?

The fastest switches tested to date are the 10-ps RPG-VCSELs above threshold. The price paid, however, is that this has required ~1 MW $cm^{-2}$ of peak optical power on the active portions of the wafer surface - this is about an order of magnitude lower than the damage thresholds of the best wafers, and represents a very heavy power requirement in practical applications. Also, the on-off switching transition time in a laser is limited by the cavity photon lifetime; any attempt to increase switching speed by shortening this lifetime results automatically in an increase in the laser threshold, hence lasers which can switch on or off in ~1 ps are difficult to justify. By using electrical biasing we can probably reduce the optical power density required for switching by two orders of magnitude while preserving the 100 GHz bandwidth potential, but the overall power density will exceed the 1 kW $cm^{-2}$ average value which is an effective upper limit for effective heat removal in quasi-CW applications. The RPA switches should be much better than this - as low as 50 W $cm^{-2}$ by our estimates - but the switching transition times will be carrier lifetime limited to a few nanoseconds.

However, the switching transition between transverse modes in a laser which remains on is limited only by carrier transport; in good quality material this can be reduced to ~1 ps in structures of reasonably size. We intend to examine the dynamics of transverse mode switching by doing an interesting series of experiments, pumping VCSEL wafers with a picosecond Ti:sapphire laser and observing the time evolution of the transverse modes by imaging the near field output onto the slit of a single-shot picosecond streak camera, as shown in Figure 27. In this way we can examine the details of transverse mode selection, stability and switching dynamics in single channels and arrays. These very fundamental experiments will be coupled with innovative theoretical studies, in collaboration with two world-renowned research groups actively involved in spatio-temporal laser dynamics. Apart from considering the implications of these spatial dynamical effects on coupled 2-D laser and switch arrays, we shall also assess the requirements for optical coupling to and from the switch arrays.

### 5.4 What do we do with optical switches, anyway?

The last suggestion for future work is to find a definite and critical use for arrays of low-threshold, gigabit optical switches. There is a definbite confusion in the field of optical switching as to what is required and what is ultimately desirable or possible. We consider the most pressing and promising application is time-multiplexing of communication or sensor channels along common fiber data buses, as illustrated in Figure 28: a series of channels derived from multiple sources (communication transmitters or sensors) is to be combined and sent over one or more fiber data buses. These buses may vary in length from ~100 km for telecommunications, to ~100 m in

**FIGURE 28**

**Time-division multiplexed arrangements of communication signals, computer data or sensor inputs (schematic).**

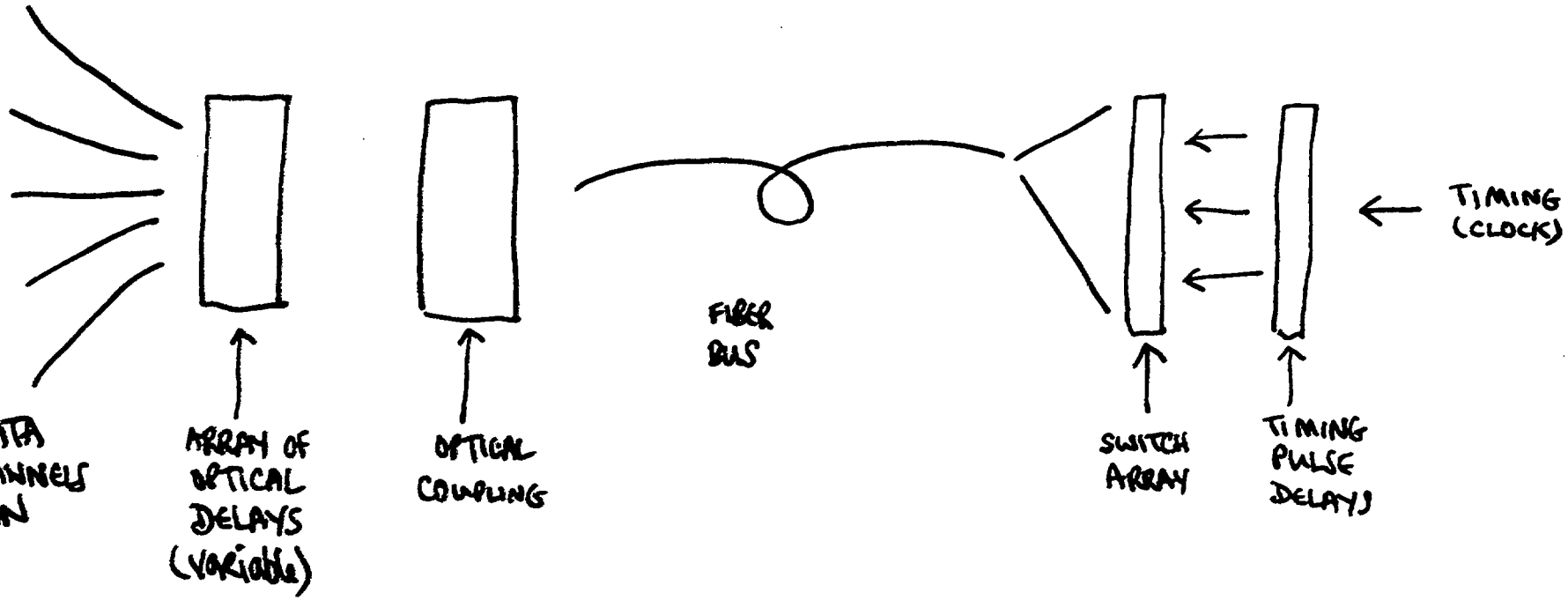


Data channels can be voice, video, computer data, sensor inputs etc. Variable delay array (e.g. fiber delays + spatial light modulator) allows initial synchronization and time slot assignment.

avionics systems, computer interconnects or short-haul communications. Each channel is assigned a time window in a synchronous data stream (one channel is designated as the clock) by insertion of fixed and variable optical delays, then the entire set of interleaved data channels is broadcast onto the switch array at the receiver.

The function of the switch array is to detect coincidences between incoming data pulses and locally-generated, clock-derived timing pulses. By setting the appropriate timing pulse delay at each switching element of the array, any given time window in the data stream may be read out by any switch, and the data demultiplexed in optical or electrical form. An artist's impression of this arrangement is given as Figure 29. Furthermore, by reconfiguring the optical delays in the timing pulses to the various switches in the array, it will be possible to reconfigure the channel assignments for data routing, multiple redundancy design *etc.* This represents a very versatile, compact, lightweight and efficient means of data highway networking in any environment from long-haul international communications to computers to airborne or space-borne platforms. It is the unique promise of the uniform, low-threshold, gigabit-per-second optical switch arrays based on RPA etalons which makes this concept feasible.

Finally, there are several interesting (and puzzling) issues which have surfaced in our picosecond optical pumping of RPG-VCSELs above threshold: what is the temporal behavior of the transverse and longitudinal coherence length? why are the optical pumping efficiencies anomalously low using picosecond pulses (compared with CW efficiencies)? are the pulse spectra (*e.g.* the chirp) suitable for further compression or amplification? These issues will be investigated vigorously in our future research on VCSEL switching dynamics.

We have just begun to appreciate the many possibilities for fundamental and applied research using resonant periodic gain/absorption structures for optical switching. These and other devices/ideas for semiconductor optoelectronic switching will be discussed and presented in more detail in a contract renewal proposal, hopefully to be presented and discussed in person by the Principal Investigator late in October 1991.

## 6 CERTIFICATION BY PRINCIPAL INVESTIGATOR

I certify that the above report is a fair and accurate representation of work performed under and associated with RADC contract F19628-89-K-0037: "*Fast optoelectronic switching processes in surface-emitting semiconductor lasers and nonlinear etalons*", at the University of New Mexico.

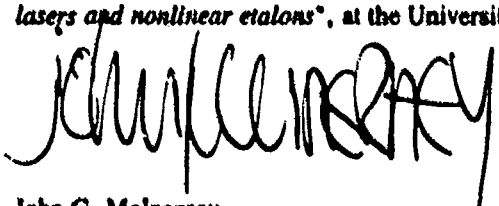

John G. McInerney
Associate Professor of Electrical and Computer Engineering
Associate Professor of Physics and Astronomy

**FIGURE 29**

**Reconfigurable time-division demultiplexing on RPA switch array by selective area coincidence detection.**

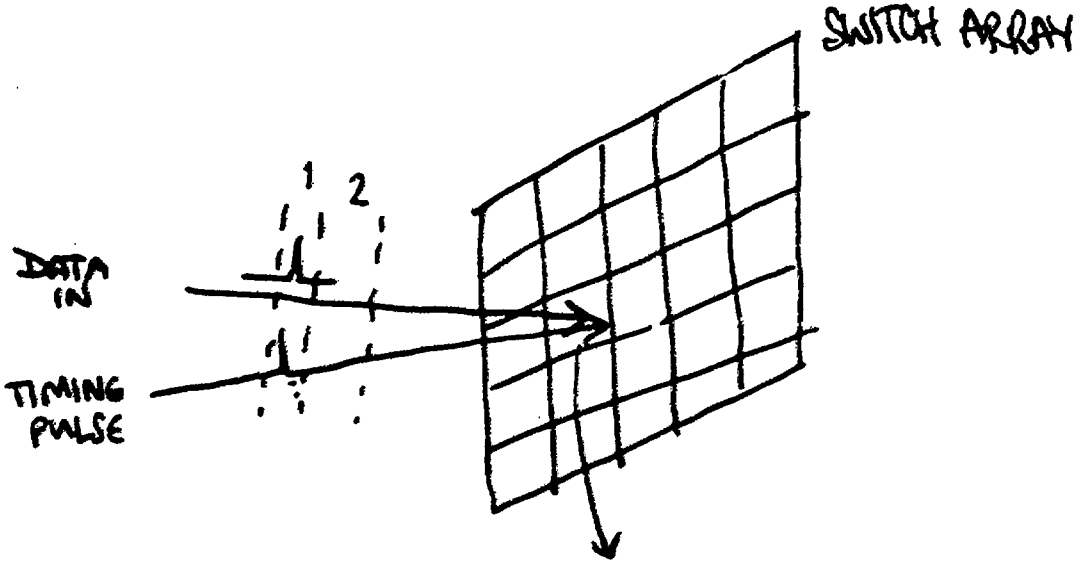


RPA configured so that both pulses required to exceed switching threshold. Electrical bias assist is optional.

Any thresholding detector array will do – RPA etalon is fast, has low threshold. Wavelength must match RPA peak.

## 7 REFERENCES


1 M. Y. A. Raja, S. R. J. Brueck, M. Osinski, C. F. Schaus, J. G. McInerney, T. M. Brennan and B. E. Hammons, "Resonant periodic gain surface-emitting semiconductor lasers," *IEEE J. Quantum. Electron.*, vol. 25, p. 1500 (1989); and C. F. Schaus, M. Y. A. Raja, J. G. McInerney, H. E. Schaus, S. Z. Sun, M. A. Mahbobzadeh and S. R. J. Brueck, "High-efficiency CW operation of MOCVD-grown GaAs.AlGaAs vertical-cavity lasers with resonant periodic gain," *Electron. Lett.*, vol. 25, p. 637 (1989).

2 S. W. Corzine, R. S. Geels, J. W. Scott, R.-H. Yan and L. A. Coldren, "Design of Fabry-Perot surface-emitting lasers with a periodic gain structure," *IEEE J. Quantum Electron.*, vol. 25, p. 1513, 1989.

3 D. L. McDaniel, J. G. McInerney, M. Y. A. Raja, C. F. Schaus and S. R. J. Brueck, "Vertical cavity surface-emitting semiconductor laser with CW infection laser pumping," *IEEE Photon. Technol. Lett.*, vol. 2, no. 3, p. 156, 1990.

4 C. F. Schaus, A. J. Torres, J. Cheng, S. Sun, C. Hains, K. J. Malloy, H. E. Schaus, E. A. Armour and K. Zheng, "Transverse junction vertical-cavity surface-emitting laser", Appl. Phys. Lett., vol. 58, p. 1736 (1991).

5 P. Zhou, J. Cheng, C. F. Schaus, S. Z. Sun, K. Zheng, E. Armour, C. Hains, W. Hsin, D. R. Myers and G. A. Vawter, "Low series resistance high-efficiency GaAs/AlGaAs vertical-cavity surface-emitting lasers with continuously graded mirrors grown by MOCVD", IEEE Photonics Techhnol. Lett., vol. 3, p. 591 (1991).

6 H. M. Gibbs, S. S. Tarng, J. L. Jewell, D. A. Weinberger, K. Tai, A. C. Gossard, S. L. McCall, A. Passner and W. Wiegmann "Room temperature excitonic optical bistability in a GaAs-GaAlAs superlattice etalon," *Appl. Phys. Lett.*, vol. 41, p. 221 (1982).

7 H. M. Gibbs, S. L. McCall and T. M. C. Venkatesan, "Differential gain and bistability using a sodium-filled Fabry-Perot interferometer," *Phys. Rev. Lett.*, vol. 36, p. 1184 (1976).

8 D. S. Chemla, D. A. B. Miller, P. W. Smith, A. C. Gossard and W. Wiegmann, *IEEE J. Quantum Electron.* vol. QE-20, p. 265 (1984).

9 H.-C. Lee, A. Kost, M. Kawase, A. Hariz, P. D. Dapkus and E. M. Garmire, *IEEE J. Quantum Electron.* vol. QE-24, p. 1581 (1988).



*U.S. GOVERNMENT PRINTING OFFICE* [illegible]

## *MISSION*

## *OF*

## *ROME LABORATORY*

*Rome Laboratory plans and executes an interdisciplinary program in research, development, test, and technology transition in support of Air Force Command, Control, Communications and Intelligence ($C^3I$) activities for all Air Force platforms. It also executes selected acquisition programs in several areas of expertise. Technical and engineering support within areas of competence is provided to ESD Program Offices (POs) and other ESD elements to perform effective acquisition of $C^3I$ systems. In addition, Rome Laboratory's technology supports other AFSC Product Divisions, the Air Force user community, and other DOD and non-DOD agencies. Rome Laboratory maintains technical competence and research programs in areas including, but not limited to, communications, command and control, battle management, intelligence information processing, computational sciences and software producibility, wide area surveillance/sensors, signal processing, solid state sciences, photonics, electromagnetic technology, superconductivity, and electronic reliability/maintainability and testability.*